Article

Cell

Enhancer Divergence and *cis*-Regulatory Evolution in the Human and Chimp Neural Crest

Graphical Abstract

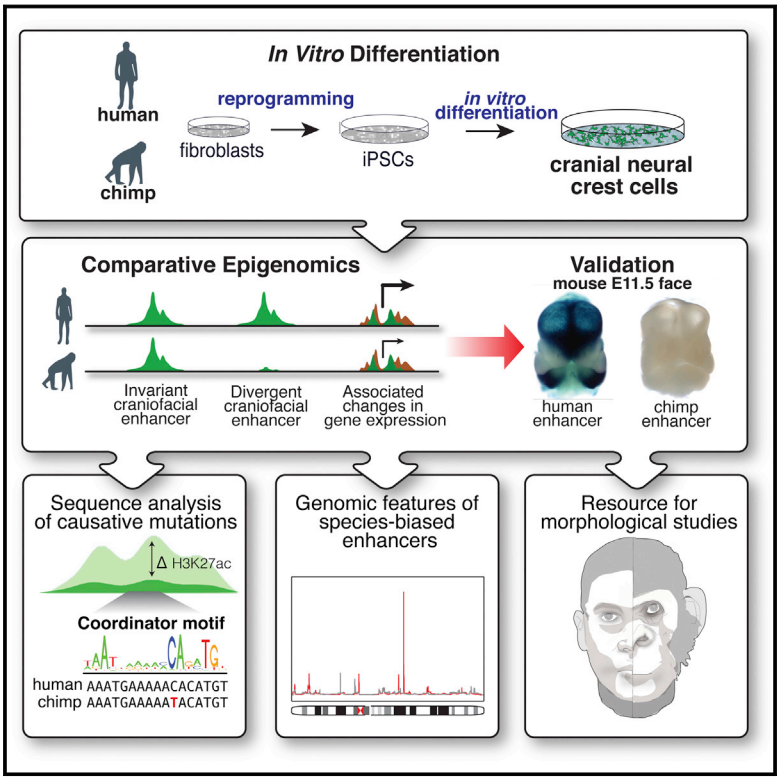

Authors

Sara L. Prescott, Rajini Srinivasan, Maria Carolina Marchetto, ..., Fred H. Gage, Tomek Swigut, Joanna Wysocka

Correspondence

swigut@stanford.edu (T.S.), wysocka@stanford.edu (J.W.)

In Brief

Epigenomic and transcriptome profiling from in-vitro-derived human and chimpanzee cranial neural crest cells (CNCCs) allows for the identification and mechanistic exploration of recent *cis*-regulatory landscape divergence underlying human craniofacial evolution.

Highlights

- Aspects of higher primate embryogenesis can be recapitulated in vitro using iPSCs
- Epigenomic profiling from human and chimp CNCCs reveals divergent facial enhancers
- Recently diverging CNCC enhancers have distinct sequence features
- Species-biased enhancers cluster near loci affecting intra-human facial variation

Accession Numbers

GSE70751

Prescott et al., 2015, Cell *163*, 68–83
September 24, 2015
http://dx.doi.org/10.1016/j.cell.2015.08.036

CellPress

Cell

Article

Enhancer Divergence and *cis*-Regulatory Evolution in the Human and Chimp Neural Crest

Sara L. Prescott,[1] Rajini Srinivasan,[1] Maria Carolina Marchetto,[2] Irina Grishina,[3] Iñigo Narvaiza,[2] Licia Selleri,[3] Fred H. Gage,[2,4] Tomek Swigut,[1,*] and Joanna Wysocka[1,5,6,*]

[1]Department of Chemical and Systems Biology and Department of Developmental Biology, Stanford University School of Medicine, Stanford, CA 94305, USA

[2]Laboratory of Genetics, The Salk Institute for Biological Studies, 10010 North Torrey Pines Road, La Jolla, CA 92037, USA

[3]Department of Cell and Developmental Biology, Weill Cornell Medical College, Cornell University, New York, NY 10065, USA

[4]Center for Academic Research and Training in Anthropogeny (CARTA), University of California, San Diego, 9500 Gilman Drive, La Jolla, CA 92093, USA

[5]Howard Hughes Medical Institute, Stanford University School of Medicine, Stanford, CA 94305, USA

[6]Institute of Stem Cell Biology and Regenerative Medicine, Stanford University School of Medicine, Stanford, CA 94305, USA

*Correspondence: swigut@stanford.edu (T.S.), wysocka@stanford.edu (J.W.)

http://dx.doi.org/10.1016/j.cell.2015.08.036

SUMMARY

cis-regulatory changes play a central role in morphological divergence, yet the regulatory principles underlying emergence of human traits remain poorly understood. Here, we use epigenomic profiling from human and chimpanzee cranial neural crest cells to systematically and quantitatively annotate divergence of craniofacial *cis*-regulatory landscapes. Epigenomic divergence is often attributable to genetic variation within TF motifs at orthologous enhancers, with a novel motif being most predictive of activity biases. We explore properties of this *cis*-regulatory change, revealing the role of particular retroelements, uncovering broad clusters of species-biased enhancers near genes associated with human facial variation, and demonstrating that *cis*-regulatory divergence is linked to quantitative expression differences of crucial neural crest regulators. Our work provides a wealth of candidates for future evolutionary studies and demonstrates the value of "cellular anthropology," a strategy of using in-vitro-derived embryonic cell types to elucidate both fundamental and evolving mechanisms underlying morphological variation in higher primates.

INTRODUCTION

Since the discovery that the protein-coding regions of the genome remain largely conserved between humans and chimpanzees, it has long been postulated that morphological divergence between closely related species is driven principally through quantitative and spatiotemporal changes in gene expression, mediated by alterations in *cis*-regulatory elements (Carroll, 2008; King and Wilson, 1975; Wray, 2007). A number of excellent case studies have validated these early predictions and demonstrated that mutations or deletions affecting distal regulatory elements called enhancers can alter ecologically relevant traits (Gompel et al., 2005; Shapiro et al., 2004; Attanasio et al., 2013). Recent successes in full-genome sequencing and epigenomic strategies have enabled the first genome-wide comparisons of transcription factor (TF) binding and regulatory landscapes in closely related species, demonstrating the value of comparative epigenomics in the context of high-genome orthology for understanding principles of *cis*-regulatory evolution (Bradley et al., 2010; He et al., 2011; Stefflova et al., 2013). Nonetheless, despite the availability of human and chimpanzee genomes, our knowledge of *cis*-regulatory divergence between humans and our closest evolutionary relatives remains fairly speculative. Previous efforts have relied heavily on computational approaches to pinpoint conserved non-coding elements that were either deleted or had undergone accelerated change specifically in the human lineage (McLean et al., 2011; Pollard et al., 2006; Prabhakar et al., 2006). Functional epigenomic comparisons between humans and other primates have been largely limited to lymphoblastoid cell lines (Cain et al., 2011; Shibata et al., 2012; Zhou et al., 2014) or to profiling whole organs from more distantly related species (Cotney et al., 2013; Villar et al., 2015).

Recently, iPSCs were made available from our nearest living evolutionary relative, the chimpanzee (Marchetto et al., 2013), offering an opportunity to derive developmentally relevant and previously inaccessible tissue types in vitro. This allows aspects of species-specific development to be recapitulated in a dish, facilitating "cellular anthropology" through the discovery of cell-type-specific regulatory changes that occurred during recent human evolution. Here, we focus on the neural crest (NC), one of the embryonic cell populations most relevant to emergence of uniquely human traits. In vivo, NC cells (NCCs) arise during weeks ~3–5 of human gestation from the dorsal part of the neural tube ectoderm and migrate into the branchial arches and what will later become the embryonic face, consequently establishing the central plan of facial morphology (Bronner and LeDouarin, 2012; Cordero et al., 2011; Jheon and Schneider, 2009). Within our recent evolutionary history, the modern human craniofacial complex has undergone dramatic changes in shape and sensory organ function, which helped to build a recognizably

human face and were required to accommodate the transition to bipedal posture, enlargement of the brain, extension of the larynx for speech, and compensatory rotations of the orbits, olfactory bulb, and nasomaxillary complex (Bilsborough and Wood, 1988; Lieberman, 1998; Spoor et al., 1994).

To overcome the inability to obtain cranial NCCs (CNCCs) directly from higher primate embryos, we here employ a pluripotent stem-cell-based in vitro differentiation model in which specification, migration, and maturation of human and chimpanzee CNCCs are recapitulated in the dish (Bajpai et al., 2010; Rada-Iglesias et al., 2012; this study). We compared TF and coactivator binding, histone modifications, and chromatin accessibility genome-wide to annotate the divergent regulatory element repertoire of human and chimpanzee CNCCs. This information allowed us to explore, with unprecedented comprehensiveness and resolution, the mechanisms of tissue-specific enhancer landscape evolution within a developmentally relevant tissue type in humans and our nearest evolutionary relative.

RESULTS

Derivation of Human and Chimpanzee CNCCs

Given the similarities in hominid gestational environment, we hypothesized that non-human primate CNCCs could be derived from pluripotent cells using the same cell culture conditions that we have previously applied to human embryonic stem cells (ESCs)/iPSCs (Bajpai et al., 2010; Rada-Iglesias et al., 2012). Chimp iPSCs have recently become available and can be maintained in vitro under identical conditions as human ESCs/iPSCs (Marchetto et al., 2013). Upon differentiation of our chimp iPSCs, we observed formation of highly mobile stellate cells that were morphologically indistinguishable from human CNCCs, expressed a broad range of migratory NC markers at levels equivalent to those seen in human cells, and had a very low level of *HOX* gene expression, a profile consistent with CNCC identity (Figures 1A-1C and S1A). To characterize staging and homogeneity of our human and chimp CNCC populations, we identified a panel of five cluster of differentiation (CD) markers, whose expression is sensitive to the developmental progression of CNCC (see Experimental Procedures and Figure S1B). These markers provided a platform for us to monitor and optimize our cell culture protocol for derivation and maintenance of primate CNCCs achieving metrics of homogeneity greater than 90% regardless of the genetic background, initial cell source (e.g., iPSC versus ESC), or species (human versus chimp); see Figure S1C and Experimental Procedures. Cultured primate CNCCs show a high correlation of expression signatures and epigenomic profiles with CNCCs isolated from chick embryos, reinforcing the NC identity of these in-vitro-derived cells (Figures S2A and S2B). Importantly, derived human and chimp CNCCs are both capable of prolonged maintenance (for up to 18 passages) and sustained differentiation capacity into both mesenchymal and non-mesenchymal lineages (Figure S2C). Furthermore, xenotransplantation of cultured human and chimp CNCCs into the dorsal neural tube of early chick embryos demonstrates their ability to engraft and then follow endogenous migration cues into the distal branchial arches (Figures S2D and S2E).

Epigenomic Profiling of Human and Chimpanzee CNCCs

For epigenomic profiling, we derived CNCCs from H9 hESCs and from iPSCs from two humans and two chimpanzees (Marchetto et al., 2013). We subsequently performed chromatin immunoprecipitation and sequencing (ChIP-seq) using antibodies against CNCC TFs (TFAP2A and NR2F1), a general coactivator (p300), and histone modifications associated with active regulatory elements (H3K4me1, H3K4me3, and H3K27ac) (Figures 1A and 1E). In parallel, we mapped genome-wide chromatin accessibility using an assay for transposase-accessible chromatin (ATAC-seq) (Buenrostro et al., 2013).

One crucial advantage of performing comparative epigenomics between human and chimpanzee, as opposed to a more distant primate relative, is the large similarity between genomes, which permits reciprocal mapping of sequencing reads to the reference genomes of both species. This allows for quantification of read enrichments from each species in the context of both reference genomes, removing otherwise difficult-to-control-for biases due to mappability, ambiguous liftOver, and other technical caveats. Importantly, we could unambiguously assign one-to-one orthology between genomes for >95% of all enhancer candidates from either species, with the remaining 4%–5% representing enhancers that fall within putative species-specific structural variants. We found that enrichments for all ChIP-ed factors and for chromatin accessibility were largely independent of the chosen reference genome and excluded all candidate elements for whom enrichment divergence was dependent upon the reference (< 0.1%) or that did not map uniquely in both genomes (see Experimental Procedures). Globally, the observed epigenomic patterns at candidate regions were highly correlated for human and chimp CNCCs (Figures 1E and Figure S4A).

Genome-wide Annotation of Human and Chimpanzee CNCC Regulatory Elements Uncovers Enhancers with Craniofacial Activity

To annotate enhancers genome wide, we promiscuously identified candidate *cis*-regulatory regions by the presence of TF or p300 enrichment and/or increased chromatin accessibility. We then restricted our analysis primarily to enhancers by assessing the ratio of H3K4me1/H3K4me3 enrichment at these candidate sites, which distinguishes distal enhancers from promoters (Heintzman et al., 2007), and further using H3K27ac enrichment to differentiate active from inactive elements (Creyghton et al., 2010; Rada-Iglesias et al., 2011). The resulting enhancer candidates had enriched conservation signatures compared to surrounding genomic regions and were near genes annotated with craniofacial ontologies—consistent with bona fide NC enhancer status (Figures S3A–S3C). Furthermore, cross-referencing our enhancer list with the VISTA Enhancer Browser database (Visel et al., 2007) identified 247 regions overlapping CNCC enhancers that were functionally tested for activity in mouse embryos. Of those 247 regions: (1) 208 were active at E11.5 (odds ratio 6.33 and $p < 5 \times 10^{-32}$), and (2) these 208 active enhancers were significantly enriched for activity in NC-derived head tissues (branchial arches and facial mesenchyme; Figure 1D, examples are shown in Figures 1E [right], and Figure S3D). Thus, our analysis captures regulatory regions relevant for distinct

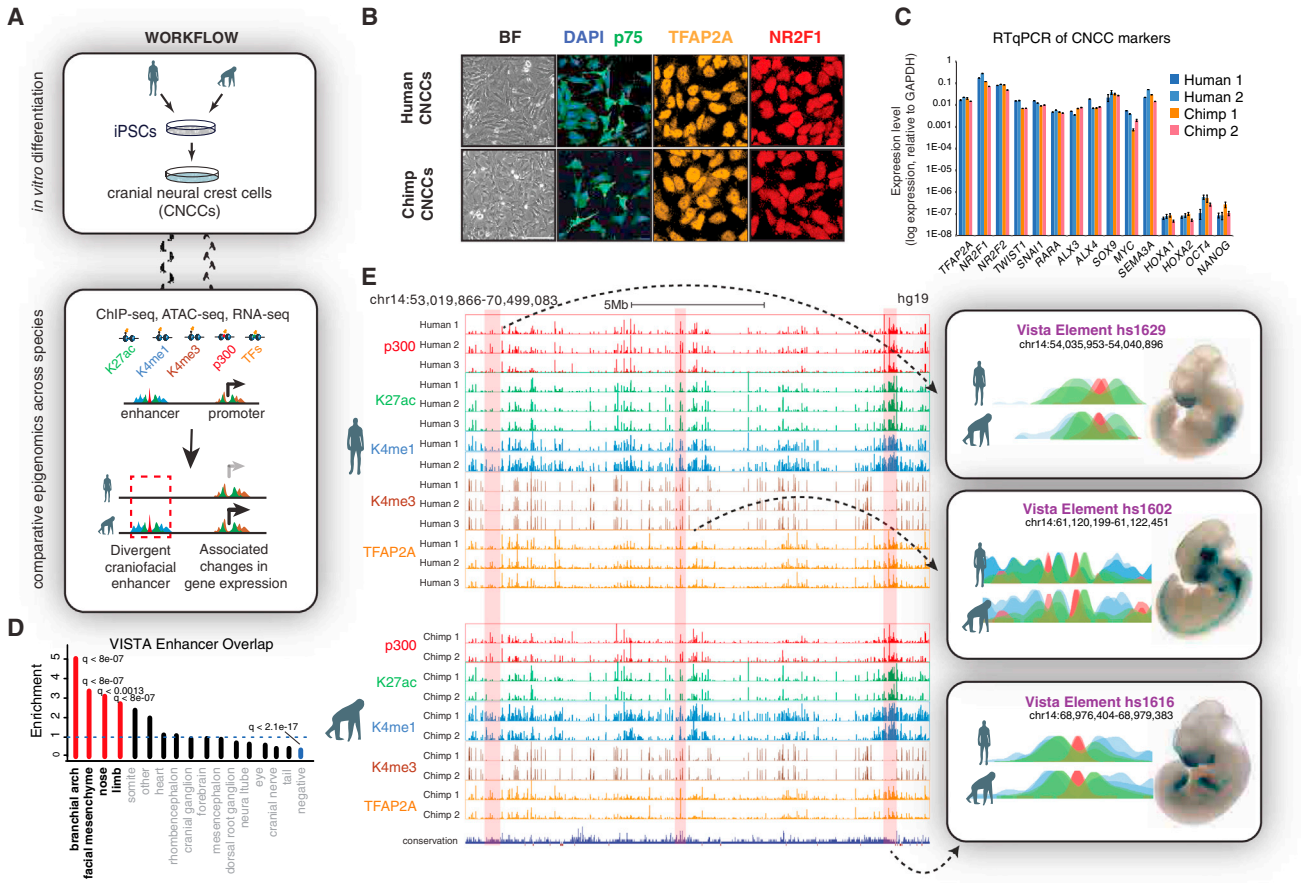

Figure 1. Derivation of Human and Chimpanzee CNCCs and Epigenomic Annotation of Craniofacial Enhancers

(A) Workflow of comparative epigenomic strategy.

(B) Confocal immunofluorescence detection of NC markers p75, TFAP2A, and NR2F1 in human and chimp CNCCs at passage 4.

(C) RT-qPCR of NC markers, HOXs, and pluripotency markers *OCT4* and *NANOG* in derived human and chimp CNCCs from two genetic backgrounds of each species. Error bars represent one SD.

(D) Enrichment of annotated expression domain categories from overlap of top 15,000 enhancer calls with regions in the VISTA enhancer database. p values were calculated with Fisher's exact test and corrected for pFDR. Categories with q value < 0.05 are indicated in red (enrichment) or blue (depletion).

(E) Representative UCSC Genome Browser tracks showing ChIP-seq profiles for p300 (red), H3K27ac (green), H3K4me1 (blue), H3K4me3 (brown), and TFAP2A (orange) from both species aligned to hg19 reference genome. Representative elements tested through the VISTA enhancer database (Visel et al., 2007) displayed on the right next to the reported *lacZ* expression domains.

spatial identities in the developing face in vivo (Figure 1D). Taken together, our epigenomic approach thus comprehensively annotates putative human and chimp NC enhancers, at least a subset of which is active in facial structures during embryogenesis.

Quantitative Analysis of H3K27ac Enrichments Predicts Species-Biased Enhancers

We hypothesized that, in closely related species, quantitative modulation of activity at orthologous regions is a major form of enhancer divergence. To identify such divergence, we used H3K27ac enrichment data in biological quadruplicate (i.e., independent CNCC derivations from each individual) to quantitatively approximate activity at all annotated CNCC enhancers detected for either species. Global comparisons of H3K27ac enrichments between individuals of the same species revealed high concordance of signals, with some minor variation due to either differences in genetic background or experimental variability (Figures 2A, highlighted in red, and S4A). Human and chimpanzee CNCC H3K27ac enrichment was also highly correlated when mapped to the same reference genome, and human and chimpanzee CNCC H3K27ac profiles clustered together distinctly from 49 other human cell types (Figures S4A and S4B). Despite this high conservation of profiles, a substantial subset of elements demonstrated a significant species bias (Figure 2A, FDR < 0.01 highlighted in blue), which we thereafter considered to be our species-biased enhancer candidates. H3K27ac ChIP-qPCR at select candidate enhancers from independent CNCC derivations recapitulated this species bias (Figure S4C).

Importantly, consistent with the premise that H3K27ac is a suitable readout of enhancer activity, the bias in H3K27ac status alone was highly predictive of biases in TF and p300 binding, as well as chromatin accessibility (Figure 2C; examples are shown

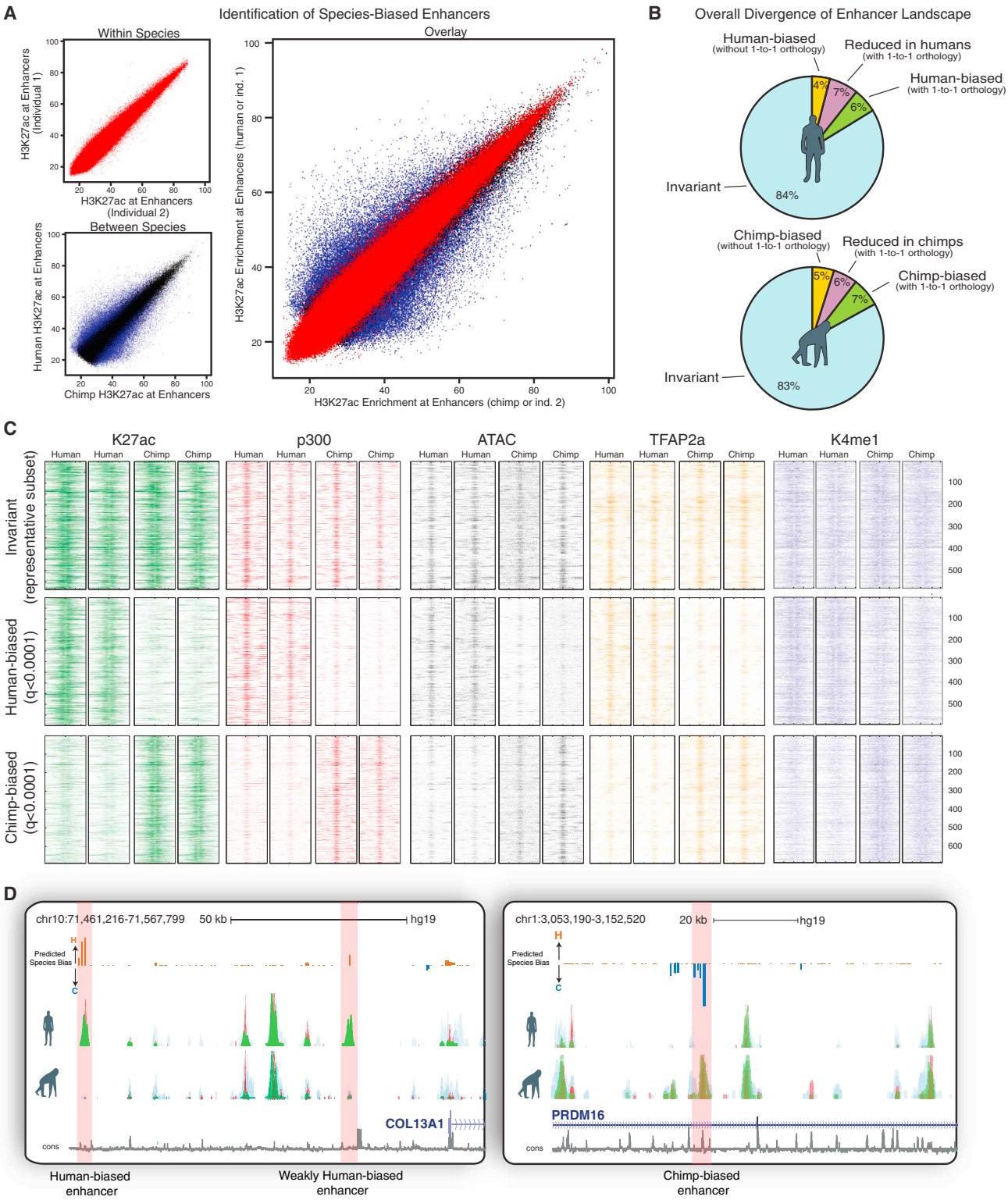

Figure 2. Identification of Species-Biased Enhancers Using H3K27ac Enrichments at Orthologous Loci

(A) Enrichment of H3K27ac at candidate enhancer elements compared within individuals of the same species (red) or across species (blue/black), with overlay shown on the right. Enhancers with significant inter-species divergence indicated in blue (p_{adj}<0.01).

(legend continued on next page)

in Figures 2D and S4D). Furthermore, this approach enabled genome-wide assignment of signed significance scores on a per-enhancer basis, visualizable as a genome browser track (Figure 2D, "Predicted Species Bias" track).

Altogether, of all annotated active human CNCC enhancers (n = 14,606), 84% were invariant, 4% fell at non-orthologous sites, and 6% and 7% demonstrated quantitative increase or decrease, respectively (Figure 2B). One limitation is the low number of currently available chimpanzee iPSC lines, especially given the high reported degree of polymorphism among chimps (Kaessmann et al., 1999). To estimate false positive rate for identifying true fixed inter-species differences, we applied our strategy to previously published ChIP-seqs from chimp lymphoblastoid cell lines and estimated a conservative FDR of 0.15 when using only two chimp genetic backgrounds. This suggests that the vast majority of identified differences represent functionally fixed differences across species (the rest represent enhancers that are still divergent but remain polymorphic within one of the species). Our observations agree with the emerging notion that quantitative modulation of enhancer activity is the prevalent source of regulatory landscape divergence among closely related species.

cis-Sequence Changes Drive Species-Biased Enhancer Activity In Vitro and In Vivo

To functionally validate our predictions, we used a luciferase reporter assay to examine activity of a selected set of orthologous pairs of species-biased human and chimpanzee enhancers. We found that >80% of tested enhancers had correlated species bias in luciferase expression, which was consistent regardless of whether the reporter assays were performed in human or chimpanzee CNCCs (Figures 3A and 3B). These results further validate that H3K27ac identifies both enhancer activity and bona fide species bias; thus, for simplicity, we refer to H3K27ac enrichment interchangeably with "activity." Importantly, these results also demonstrate that enhancer divergence can be largely explained by *cis*-sequence changes rather than differences in the *trans* regulatory environments of the human and chimp CNCCs.

The conservation of *trans*-environments across species facilitates testing of human and chimp regulatory elements in vivo using a mouse LacZ transgenic reporter assay. We selected two predicted human-biased enhancers near *CNTNAP2* (enhancer 1) and *PAPPA* (enhancer 2), respectively (Figures 3C and 3D). For both predicted human-biased enhancers we observed gains of additional expression domains in head regions, as well as quantitative gains in enhancer strength, as evidenced by the overall higher LacZ staining intensity for the human sequence compared to the chimp ortholog (Figures 3C–3H and S5). Notably, to ensure that the negative/weak staining results obtained with the chimp sequences were not a result of undersampling, we performed surplus embryo injections with both chimp enhancer reporters (Figure S5A). Thus, species-biased enhancers identified in our in vitro analysis drive distinct expression patterns within CNCC-derived tissues in vivo.

Human Accelerated Regions Overlap with Distal CNCC Enhancers

Our results suggest that DNA sequence is the predominant driver of enhancer divergence; therefore, we began examining sequence properties of species-biased enhancers. Although species-biased enhancers were similar in H3K27ac enrichment levels when compared to invariant enhancers, they showed a distinct reduction of sequence conservation signatures (Figure 4A). Furthermore, we identified 163 "human accelerated regions" (HARs; Hubisz and Pollard, 2014) overlapping active chromatin features in CNCCs, of which 20 showed species-biased activity (at a cutoff of $q < 0.001$; n = 48 with a cutoff of $q < 0.1$) (Figures 4B and S6A–S6D), representing a significant enrichment relative to the whole enhancer set ($p < 0.025$, odds ratio 1.81). It is possible that the HAR-overlapping regions without species bias in CNCC could manifest divergence in another tissue type, as exemplified by HAR2 (a.k.a., HACNS1), which overlaps an invariant CNCC enhancer (Figure S6D, p value of species bias = 0.339) that has a pharyngeal arch activity domain that is conserved in primates but has human-specific activity in the embryonic limb (Prabhakar et al., 2008).

Species-Biased Enhancers Are Enriched for Specific Classes of Retroelements

Given that nearly half of the human genome is composed of transposable elements, the majority of which invaded the primate lineage prior to the separation of humans and chimpanzees (Cordaux and Batzer, 2009), we hypothesized that a subset of species-biased orthologous enhancers may be transposon derived. Interestingly, we found that, while CNCC enhancers overlapped with many different classes of repeats, specific subclasses of endogenous retroviruses (ERV1, ERVL-MaLR, and ERVK) as well as L1 elements were preferentially enriched at species-biased enhancers (Figure 4C), suggesting that these specific subclasses may harbor progenitor sequences that are prone to acquire CNCC enhancer activity over relatively short evolutionary distances.

(B) Pie charts showing the percentage of total active CNCC enhancers classified as either species-biased enhancers with gained activity (green), species-biased enhancers with decreased activity (purple), enhancers without clear orthology across genomes (yellow), or invariant enhancers (blue) using a human reference genome (above) or chimp reference genome (below).

(C) Heatmap of raw ChIP-seq and ATAC-seq counts across species-biased and invariant CNCC enhancers for two human and two chimp genetic backgrounds. Each row represents a 2 kb window (1 kb each direction) centered around the middle of human-biased (n = 598, $q < 0.0001$), chimp-biased (n = 691, $q < 0.0001$), or invariant (n = 584 representative subset, $q > 0.95$) enhancers for H3K27ac (green), p300 (red), TFAP2A (yellow), K4me1 (blue), and ATAC-seq (gray). All reads were aligned to hg19.

(D) Representative browser tracks showing overlaid H3K4me1 (blue), p300 (red), and H3K27ac (green) from human and chimp CNCCs mapped to hg19. Examples of strongly human-biased, weakly human-biased, or strongly chimp-biased enhancers highlighted in pink. Predicted species-bias track shown above for candidate enhancers; the magnitude of the bias track represents −log10 (adjusted p value of divergence) with negative sign (indigo) representing chimp bias and positive (bronze) human bias.

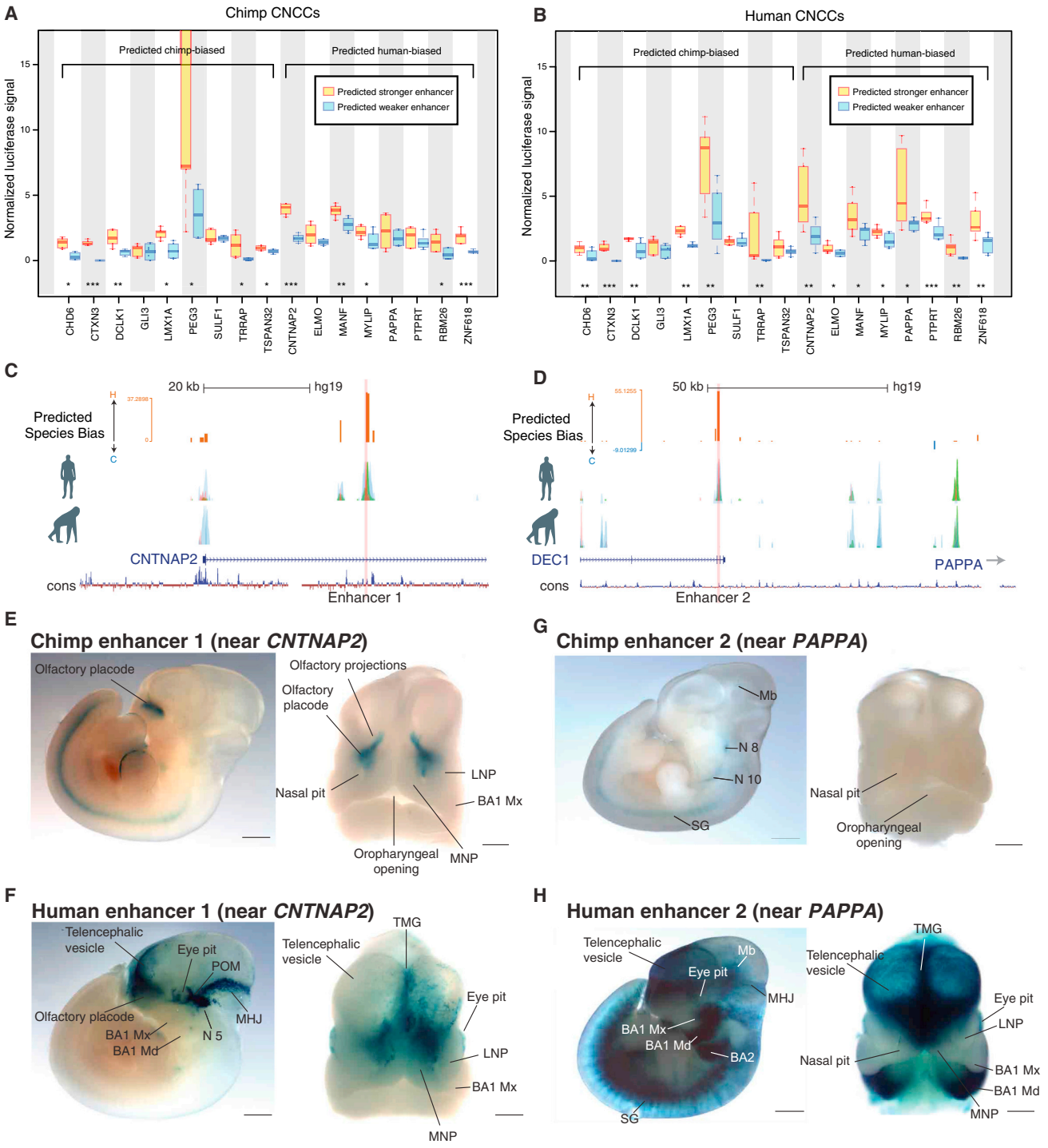

Figure 3. In Vitro and In Vivo Validations of Species-Biased Enhancers

(A and B) Luciferase reporter assays performed in chimp CNCCs (A) or human CNCCs (B) for 9 chimp-biased regions (and orthologous human regions) and 8 human-biased regions (and orthologous chimp regions). Luciferase signal was normalized to renilla transfection control. Significance tested from three biological replicates from each species with ANOVA followed by residuals testing with Student's t test. *$p < 0.05$, **$p < 0.01$, ***$p < 0.001$. Central bar represents the median, box outline represents first and third quartile, and whiskers extend to furthest datapoint within 1.5× box length way from the box. Tested enhancers are named by nearest gene.

(C and D) Genome browser tracks showing human-biased enhancer 1 (near *CNTNAP2* gene; C) and enhancer 2 (near *PAPPA* gene; D) selected for a *lacZ* reporter mouse transgenesis assay.

(E and F) Analysis of enhancer activity for chimpanzee and human enhancer 1 in a *lacZ* reporter transgenic mouse assay. (E) Representative E11.5 transgenic embryo obtained for the chimpanzee enhancer 1 reporter, shown in lateral view (left) or frontal view (right) of the embryonic head. (F) Representative E11.5

(legend continued on next page)

Sequence Substitutions within TF Binding Motifs at Species-Biased Enhancers Contribute to Epigenomic Divergence

Consistent with the expectation that species-specific biases are largely sequence driven, we observed that the variance in H3K27ac between species at each enhancer scales proportionally with the degree of sequence dissimilarity (i.e., Levenshtein distance) at those orthologous sites, while the intra-species variance at the same regions remains unchanged (Figure 4D). Nonetheless, even at enhancers with detectable species bias, sequence substitutions were still infrequent—only ~3–6 substitutions per 500 bp enhancer—suggesting that a small number of mutations can confer substantial effects on overall enhancer activity, likely by affecting binding of key sequence-dependent TFs. We therefore interrogated how frequently sequence substitutions fall within particular classes of TF motifs and to what degree these mutations correlate, either positively or negatively, with changes in enhancer activity or other chromatin modifications (Figure 4E). This, in essence, leverages preexisting genetic variation like a large-scale mutagenesis screen.

Through this approach, we identified a large set of both known and novel motifs for which deviation from the consensus was correlated with species bias of H3K27ac and other epigenomic marks, implying functional consequences for these mutations. As expected, the correlations vary in frequency and in effect, with some motifs being frequent and having small effects (e.g., Forkhead factors) and others being infrequent but conferring large effects (e.g., TFAP2A), with one outlier motif being both very frequent and conferring large effects when mutated (see description of the ''Coordinator'' motif below) (Figure 4F). Among our top hits, we identified many motifs for TFs with known effects in NC regulation, including a set of TFAP2 motif variants that serve as a positive control for our approach, as we see a high correlation between TFAP2 motif mutations and inter-species divergence in TFAP2A ChIP signals at these sites (Figure 4G, group 3). We previously showed that TFAP2A participates in establishment of active chromatin states at NC enhancers (Rada-Iglesias et al., 2012), and consistently we observed that divergence from the TFAP2A consensus also correlates with the loss of H3K27ac, co-activator binding, and chromatin accessibility. Notably, TFAP2 motifs are depleted from species-biased sites, likely due to strong selective pressure to conserve TFAP2A function in the NC and possibly in other pleiotropic contexts (Figure 4F). Another interesting set of motifs, which are both frequent at species-biased sites and positively correlated with permissive chromatin states, are those recognized by ALX homeobox factors that are highly expressed in the face and mutated in severe frontonasal dysplasias in humans (Twigg et al., 2009) (Figures 4F and 4G, group 2).

Intriguingly, we also identified a group of motifs whose mutations away from the consensus were correlated with a gain in chromatin accessibility and H3K27ac, suggesting that these motifs may recruit repressive factors with negative effects on overall enhancer activity. Examples of such motifs included the SNAI2 motif, which is bound by a known transcriptional repressor, the TBX family motif bound by T-box factors, and other candidate negative regulators representing distinct TF classes, e.g., HIC1/2, MESP1, TCF3/4, and GLIS1 (Figure 4G, group 1). These results suggest an unappreciated prevalence of repressive inputs in quantitative modulation of enhancer activity.

"Coordinator": A novel Motif that Is Highly Predictive of Active Chromatin States and Species Bias

Surprisingly, one motif stood out as an outlier in this analysis, as it was exceptionally enriched at divergent sites and was the most correlated with changes in all examined active chromatin features (Figures 4F, upper-right, and 4G, far-right). This sequence, which we termed the ''Coordinator'' motif, is a 17-bp-long motif, which we identified through de novo motif discovery from our CNCC-specific enhancers and was not previously annotated to a known regulatory complex. We note that portions of the Coordinator resemble an E box and HOX-like motifs; however, these represent large protein families, and the particular factors that bind at this element remain to be identified.

Sequence analysis using INSIGHT, a tool to infer signatures of recent natural selection using human polymorphism data (Gronau et al., 2013), found evidence of positive selection at the Coordinator motif occurrences within species-biased enhancers, but not within invariant enhancers, suggesting that the motif and its cognate binder(s) have played a privileged role in recent enhancer divergence in primate CNCCs (Figure 5A). When we further dissected the motif by individual bases, we found that the correlations of each nucleotide with ChIP enrichments (both for histone modifications and TF ChIPs) recapitulated the information content of the motif itself, as would be expected if Coordinator motif mutations were causal for the observed chromatin changes (Figure 5B). Fittingly, we found human mutations that strengthen the Coordinator motif within both human-biased enhancers tested in mouse transgenesis (Figure S6E). Globally, the Coordinator motif was preferentially enriched at distal regulatory elements rather than at promoters (Figure S6F) and was further enriched at enhancers that were CNCC specific as opposed to those that shared measurable H3K27ac in other tissue types (Figure 5C). Interestingly, we observe that LTR9 elements, a retroelement class enriched at species-biased enhancers, are 5× more likely to harbor a Coordinator motif variant than MER52A elements, a similar repeat

transgenic embryo obtained for the human enhancer 1 reporter, shown in lateral view (left) or frontal view (right). Midbrain/hindbrain junction (MHJ); periocular mesenchyme (POM); lateral and medial nasal processes (LNP and MNP); maxillary (Mx) and mandibular (Md) processes of branchial arch 1 (BA1) and BA2. Scale bars: 100 μm (left images) and 50 μm (right images).

(G and H) Analysis of enhancer activity for chimpanzee and human enhancer 2 in a *lacZ* reporter transgenic mouse assay. (G) Representative E11.5 transgenic embryo obtained for the chimpanzee enhancer 2 reporter, shown in lateral view (left) or frontal view (right) of the embryonic head. (H) Representative E11.5 transgenic embryo obtained for the human enhancer 2 reporter, shown in lateral view (left) or frontal view (right). Midbrain (Mb); cranial nerves 8 and 10 (N8 and N10 respectively); sympathetic ganglia (SG); telencephalic midline groove (TMG); midbrain/hindbrain junction (MHJ); maxillary (Mx) and mandibular (Md) processes of branchial arch 1 (BA1) and BA2. Scale bars: 100 μm (left images) and 50 μm (right images).

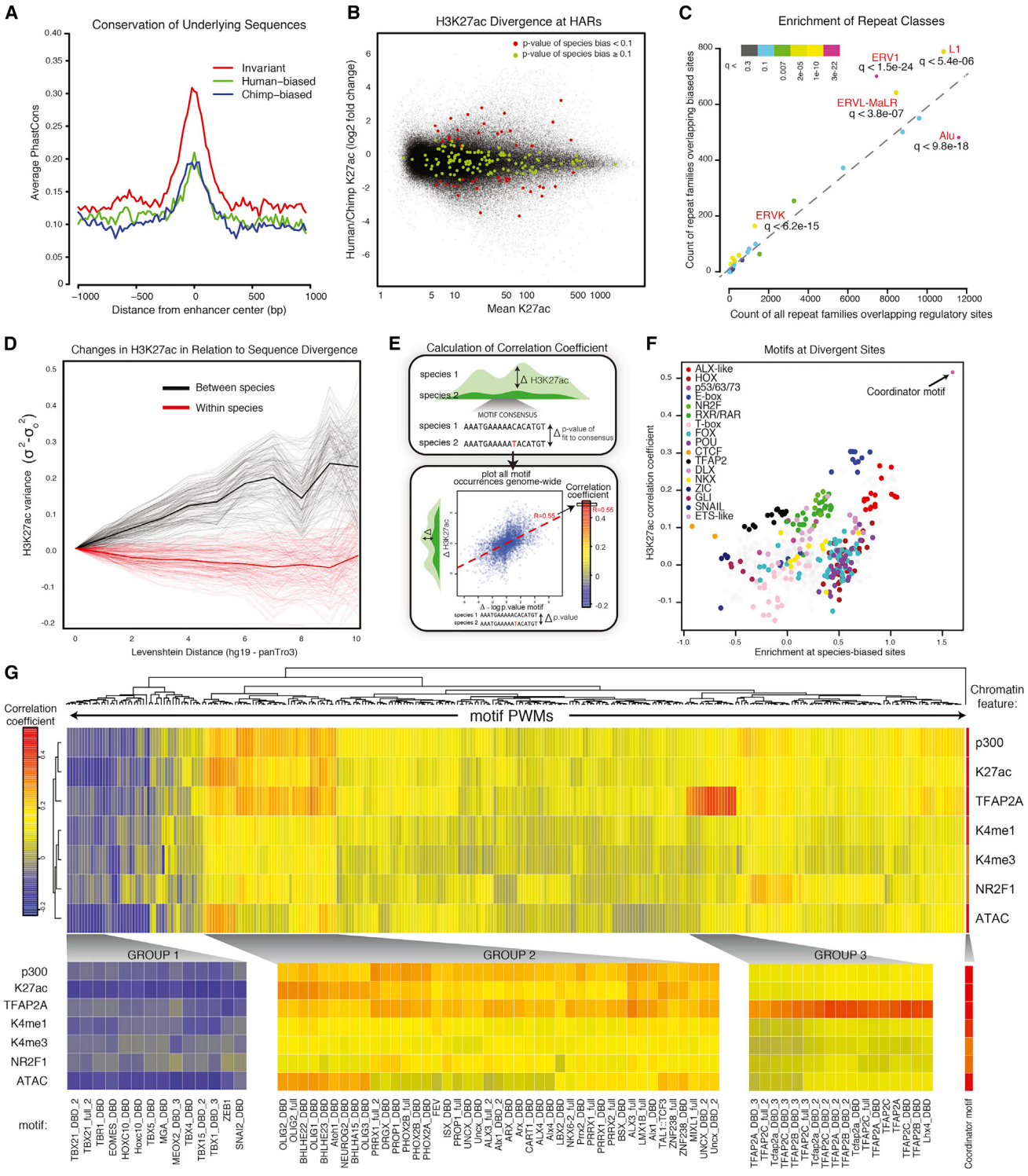

Figure 4. Global Features of Species-Biased Enhancers and Correlation of Mutations within TF Binding Motifs with Epigenomic Divergence

(A) Average PhastCons scores are shown for strong invariant enhancers (q > 0.98), strongly human-biased enhancers (q < 0.0001), or strongly chimp-biased enhancers (q < 0.0001) for 1 kb surrounding each enhancer center.

(B) Degree of species bias (log_2 fold change H3K27ac human/chimp, y axis) relative to enhancer strength (human-chimp-averaged H3K27ac enrichment, x axis) for bulk CNCC elements (black) and elements overlapping HARs (color representing q value of species bias: q < 0.1 in red, q ≥ 0.1 in green).

(C) Counts of repeat families overlapping species-biased enhancers (y axis) relative to counts of repeat families overlapping all CNCC regulatory sites (x axis) are plotted. q values of enrichment for different repeat classes is indicated by color.

(legend continued on next page)

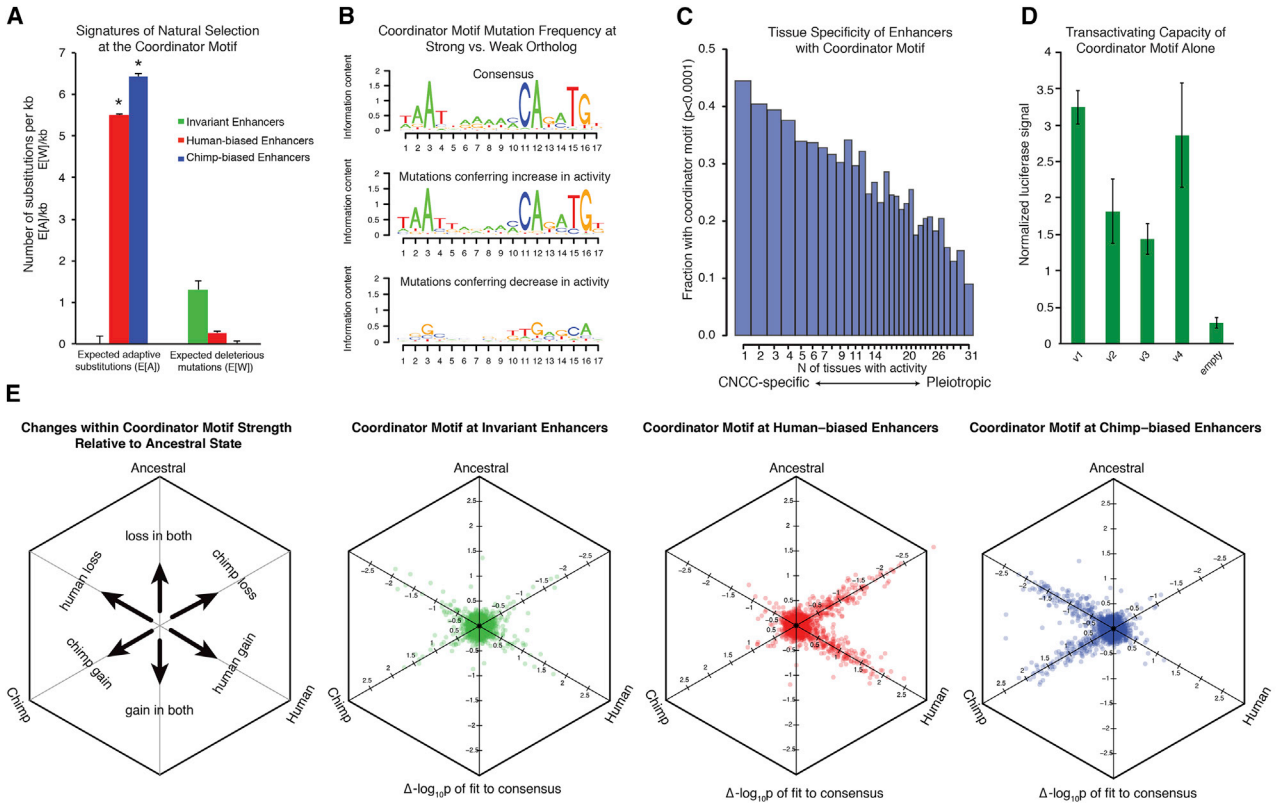

Figure 5. Properties of the Novel "Coordinator" Motif

(A) Expected number of adaptive substitutions (E[A]) per kilobase and expected number of deleterious mutations E[W] per kilobase were calculated for all sites of the Coordinator motif at invariant enhancers (green), at human-biased enhancers (red), and at chimp-biased enhancers (blue) using default INSIGHT parameters (Gronau et al., 2013). Significance indicated by * ($p < 0.01$). Overall fractions of nucleotides under selection (ρ) not shown ($\rho_{\mathbf{invariant}} = 0.66$, $p < 0.01$; $\rho_{\mathbf{human\text{-}biased}} = 0.015$, $p < 0.01$; $\rho_{\mathbf{chimp\text{-}biased}} = 0.019$, $p < 0.01$). Error bars represent approximate SE.

(B) Position weight matrix of the Coordinator consensus sequence from top 3,000 CNCC specific enhancers is shown (top) relative to logo of mutations preferred at more acetylated (H3K27ac) alleles (middle) versus mutations at less acetylated alleles (bottom).

(C) Enhancers were scored for H3K27ac ChIP-seq enrichments from 30 public data set cell types and binned by number of tissues with activity (1 to 31). The fraction of enhancers per bin with recognizable Coordinator motif ($p < 0.0001$) is indicated on y axis.

(D) Four different versions (V1–V4) of the Coordinator motif were cloned in tandem into luciferase reporter vectors and were tested for transactivation activity in human CNCCs. Luciferase was normalized relative to renilla transfection control. Error bars represent one SD.

(E) Comparison of sequence changes within the Coordinator motif with a reconstructed human-chimp ancestral outgroup. Changes in fit to the Coordinator consensus compared to the ancestral ortholog ($-\log_{10}$ p value) were plotted as orthographic projections along space diagonals for all occurrences of the motif for both human and chimpanzee lineages at different classes of sites. Overlapping data points were jittered for better visualization. Schematic is shown on the far left.

class depleted from species-biased sites. Even at sites without activity in CNCCs, LTR9 sequences are 3.7× more likely to harbor a Coordinator-like motif than MER52A, consistent with the idea that a preexisting Coordinator-like progenitor sequence contributed to the recent adaptation of some retroelements for CNCC enhancer function. Lastly, we found that the Coordinator motif alone was able to drive activity in luciferase reporter assays in CNCCs (Figure 5D).

(D) Pairwise H3K27ac variance $\sigma 2\text{-}\sigma 2_{ld\ =\ 0}$ at enhancers across samples, ranked by increasing sequence dissimilarity counted by Levenshtein distance (ld) between human (hg19) and chimp (panTro3) orthologous 200 bp enhancers, relative to ld = 0. Comparison between samples of different species shown in black; same species shown in red (means represented by thick lines).

(E) Schematic showing method for deriving the correlation coefficient. For a given motif, each occurrence genome wide containing a genetic change across species is plotted as Δ-log10 p value (human/chimp) of the fit to consensus (x axis) versus ΔH3K27ac for the overlying enhancer region (human/chimp) (y axis), then a line is fit. The slope of the line represents the correlation coefficient for that given motif and epigenomic modification genome wide.

(F) Enrichments of classes of motifs at species-biased enhancers over all enhancers (log odds ratio, x axis) plotted relative to genome-wide correlation coefficient calculated for each motif (using H3K27ac), as described in E (y axis).

(G) Genome-wide correlation coefficients were calculated for whole databases of annotated motifs and multiple chromatin features, revealing motifs with large influence on epigenomic profiles. Correlation coefficients are bi-clustered per motif, and resulting changes in enrichment of chromatin features (p300, K27ac, TFAP2A, H3K4me1, H3K4me3, NR2F1, ATAC) at all enhancers containing mutated PWMs are represented by color. Individual subclusters are magnified below with corresponding motifs indicated.

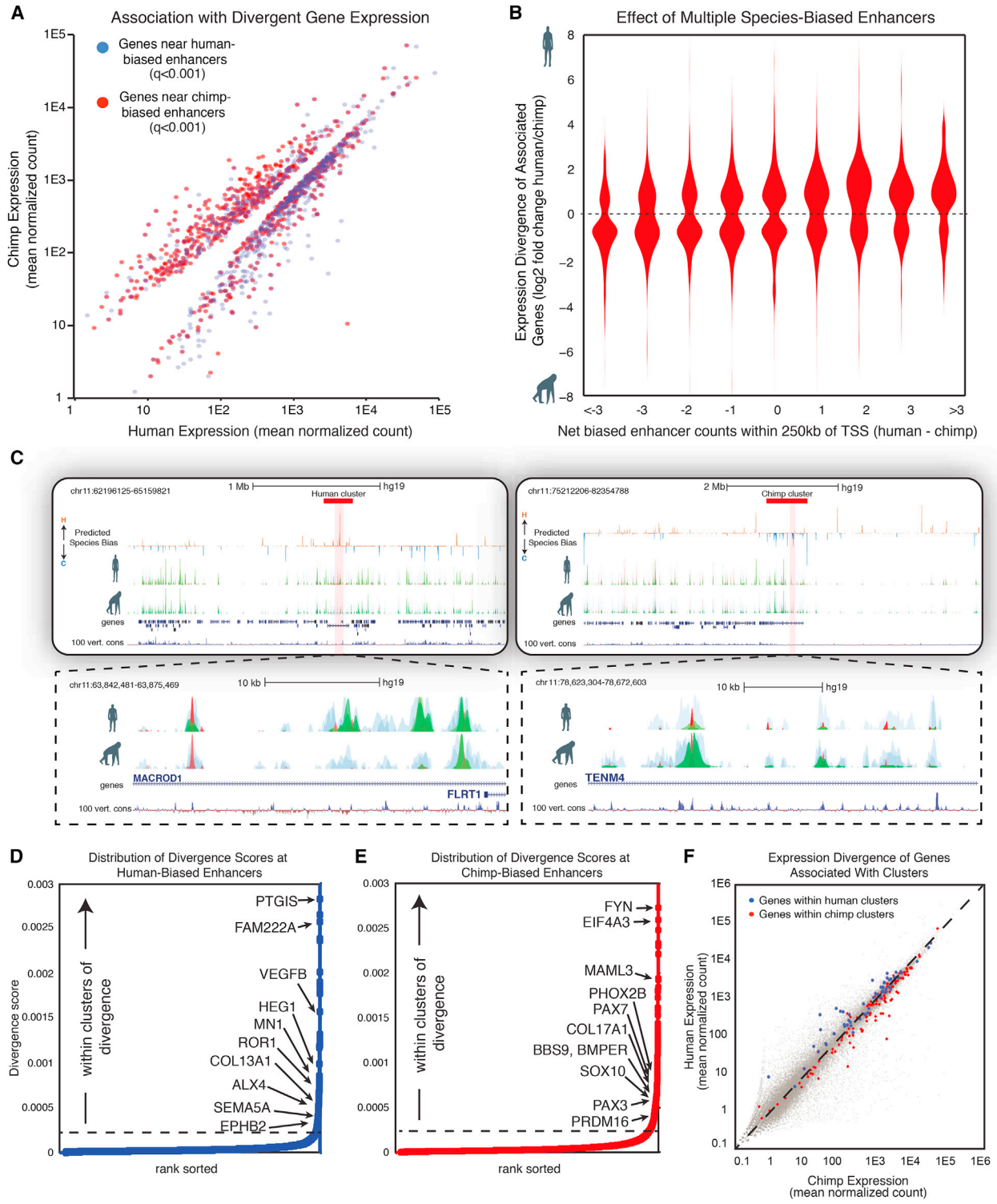

Figure 6. Clusters of Regulatory Divergence Overlap Loci with Crucial Roles in Trait Variation and Are Predictive of Expression Bias

(A) Mean normalized human expression (x axis) versus mean normalized chimp expression (y axis) for genes associated with human-biased enhancers ($q < 0.001$, blue) or with chimp-biased enhancers ($q < 0.001$, red). Only genes with significant inter-species expression change (p_{adj} value < 0.1) are shown.

(B) Violin plots showing $\log_2$ fold change human/chimp H3K27ac enrichment at orthologous enhancers binned by total count of biased enhancers (total number of human-biased enhancers minus total number of chimp-biased enhancers) within 250 kb of promoter regions for genes with significant differences in expression across species (p_{adj} value < 0.1).

(legend continued on next page)

Sequence Analysis Reveals the Recent Evolutionary History of Coordinator Motif Changes

Our results suggest that nucleotide changes within Coordinator motif sites represent an important class of "causative" mutations predictably associated with gain or loss of CNCC enhancer activity. Thus, by comparing the fit to the consensus for Coordinator-like motifs with a reconstructed ancestral outgroup, we can infer the polarity of enhancer activity change in each lineage relative to the common human-chimp ancestor. Using this strategy, we observed that human-biased enhancers contain Coordinator-like sequences that were equally prone to: (1) a gain in the fit in the human lineage (n = 300) or (2) a loss in the fit in the chimp lineage (n = 255) relative to the ancestral state (Figure 5E). However, human-biased enhancers contain almost no examples in which there was a gain of Coordinator fit in the chimp lineage or loss in the human lineage, an important validation of our analysis. Conversely, we see that chimp-biased enhancers are similarly prone to gains of the Coordinator motif in the chimp lineage (n = 218) versus losses in the human lineage (n = 255) and again, with almost no gains in human or losses in chimp. Thus, there appears to be no preferred direction of enhancer divergence in either lineage since the split from our common ancestor for this class of sites. We also applied our analysis to hominin outgroups such as Denisovans and Neanderthals and found that, as expected given the much more recent split from the common ancestor, these lineages primarily share the human-like variants of the Coordinator motif at species-biased sites (Figure S6G). Therefore, even for individuals substantially more diverged than any modern human, most changes are present in the hominin lineage relative to the human-chimp ancestor. However, there is a small set of changes that are unique to modern humans compared to other hominins, and those clearly merit further exploration.

Species-Biased Enhancers Flank Genes that Show Species-Biased Expression

Recent studies suggest that gene expression levels are more evolutionarily conserved than utilization of *cis*-regulatory elements and can be buffered by redundant or compensatory elements regulating the same loci (Hong et al., 2008; Odom et al., 2007; Schmidt et al., 2010; Vierstra et al., 2014; Wong et al., 2014). Nonetheless, at least some of the species-biased enhancers should be associated with transcriptional changes at nearby genes if they are responsible for morphological variation. To test this, we performed RNA-seq analyses of our human and chimp CNCC populations and identified genes whose expression significantly diverged between, but not within, species. We found that genes with significantly divergent expression between humans and chimpanzees are strongly enriched for nearby species-biased enhancers, with human-biased genes flanked by human-biased enhancers and chimp-biased genes flanked by chimp-biased enhancers (Figure 6A). In addition, we observed that the fraction of species-biased genes (but not the degree of the expression bias) scales with the number of flanking enhancers biased toward the same species (Figure 6B).

Clusters of Regulatory Divergence Flank Loci Involved in Intra-Human Facial Variation

Interestingly, we found that strongly divergent enhancers were not distributed at random throughout the genome but instead were likely to fall in close genomic proximity to other species-biased enhancers matching in polarity (Figure S7A), suggesting that divergent enhancers fall into regulatory clusters. To systematically locate these clusters, we calculated a genome-wide divergence score using a moving window over the nearest ~10 enhancers for each species, integrating both the degree and genomic span of divergent enhancers in series (Figure S7B). This strategy revealed a low baseline encompassing the bulk of interspersed species-biased enhancers (examples of Chr11 in Figures S7C and S7D, top) but exposed a subset of regions throughout the genome (~1–4 per chromosome), with a marked increase in their divergence score resulting from presence of dense clusters of strongly biased enhancers (Figure 6C). Importantly, we find that these clusters of divergence do not emerge simply by chance due to increased frequency of enhancers near highly active CNCC genes (Figures S7C and S7D).

When ranking all human- and chimp-biased enhancers according to their divergence score, we observed an inflection in the distribution (Figures 6D for human, 6E for chimp). Using this inflection point as a cutoff, we identified 32 human and 65 chimp clusters of divergence, spanning genomic windows of, on average, ~500 kb and encompassing ~11.9% of all species-biased enhancers. Of note, while some clusters overlapped super-enhancers in CNCCs, most super-enhancers were not identified as a species-biased cluster and many species-biased clusters did not encompass super-enhancers, indicating that these two entities are distinct (Whyte et al., 2013).

We speculate that these species-biased enhancer clusters represent broad *cis*-regulatory regions under strong evolutionary pressure to diverge and hypothesize that they may contain genes with central roles in the regulation of NC-associated phenotypes. Indeed, these regions fall immediately over or next to genes that are critical in facial morphogenesis, including *PRDM16*, *MN1*, *COL17A1*, *EDNRA*, *PAX3*, *PAX7*, *SOX10*, and *ALX4*. Intriguingly, of five chromosomal regions linked to normal-range human facial variation in GWAS, three (*PRDM16*, *COL17A1*, and *PAX3*) fall directly within these regions of high divergence. Importantly, the clusters were highly predictive of changes in nearby gene

(C) Representative browser tracks showing clusters of species-biased enhancers. Top panel shows broad view with predicted species-bias track (human-biased in orange, chimp-biased in blue) and the corresponding H3K4me1 (blue), p300 (red), and H3K27ac (green) from two individuals of each species shown in overlay. Boundaries of the cluster are indicated by a red block. Close-up of an individual cluster of biased enhancers is shown below. All chromatin features are mapped to hg19.

(D and E) Distribution of divergence scores at human-biased enhancers (D) and chimp-biased enhancers (E). Selected genes falling within identified clusters are highlighted next to the enhancer in the cluster with highest divergence score.

(F) Mean normalized human expression (x axis) versus mean normalized chimp expression (y axis) for genes within or flanking human-biased enhancer clusters (blue) or chimp-biased enhancer clusters (red).

A

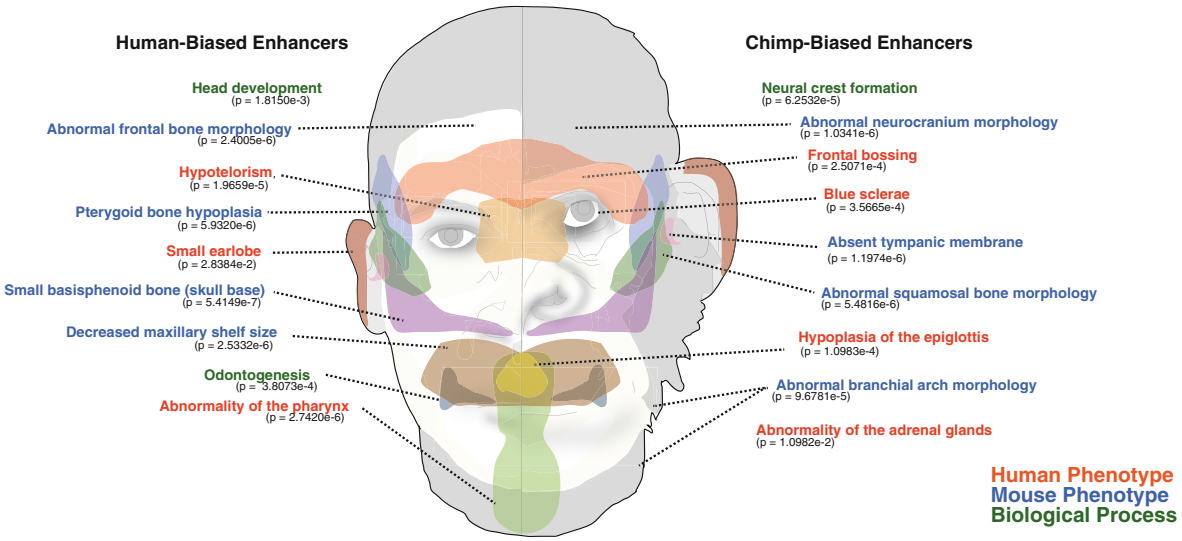

B

Gene	Expression bias:	DESEQ q value	Coordinates of nearby species-biased enhancers (hg19)	Relevant genetic phenotypes, disease associations and comments	References
PAX3	C	4.1584E-06	chr2:223983203-223983402; chr2:223157099-223157298 ; chr2:223148418-223148617 ; chr2:223084744-223084943 ; chr2:223006007-223006206 ; chr2:223005367-223005566; (see Figure S4B);	Heterozygous loss-of-function mutations cause Waardenburg syndrome, characterized by craniofacial, auditory and pigmentation defects; in model organisms Pax3 is involved in induction, specification and differentiation of neural crest cells and craniofacial development; in GWAS studies the locus was associated with normal-range variation of facial morphology in Europeans.	Asher et al., 1996; Conway et al., 1997; Liu et al., 2012; Milet et al., 2013; Paternoster et al., 2012; Tassabehji et al., 1992; Tremblay et al., 1995;
PAX7	C	0.11724596	chr1:19267843-19268042 ; chr1:19268294-19268493 ; chr1:19268848-19269047 ; chr1:19271215-19271414 ; chr1:19275542-19275741 ; chr1:19276342-19276541	Involved in early specification of the neural crest in the embryo; loss of function in the mouse leads to reduction of the maxilla and a pointed snout.	Basch et al., 2006; Mansouri et al., 1996;
EDNRA	C	1.1308E-04	chr4:148262113-148262312; chr4:148276381-148276580 ; chr4:148454528-148454727 ; chr4:148455160-148455359 ; chr4:148507330-148507529 ; chr4:148508238-148508437; chr4:148510911-148511110 (see Figure S4B);	Mouse deficient for Ednra exhibit cranial and cardiac neural crest defects. Most lower jaw structures in Ednra$^{-/-}$ embryos undergo a homeotic transformation into maxillary-like structures; other defects include absence of tympanic rings, malleus, and incus, and the rostral relocation of the hyoid bone.	Clouthier et al., 1998, 2010; Ruest et al., 2004
EDN3	H	5.2338E-03	chr20:57723838-57724037 ; chr20:57724804-57725003 ; chr20:57726203-57726402 ; chr20:57894099-57894298 ; chr20:57988186-57988385 ; chr20:58028164-58028363 ; chr20:58028993-58029192 ; chr20:58154612-58154811 (see Figure S4B);	Heterozygous or homozygous mutations associated with several human neurocristopathies, including Waardenburg syndrome type 4B, Hirschprung's disease, and Congenital Central Hypoventilation Syndrome (CCHS); in animal models EDN3 is involved in the regulation of coat pigmentation and enteric neuron function.	Baynash et al., 1994; Bidaud et al., 1997; Dupin et al., 2000; Edery et al., 1996; Lahav et al., 1996; Pingault et al., 2001;
NRP2	H	4.7551E-02	chr2:206515229-206515428 ; chr2:206436082-206436281 ; chr2:206266143-206266342 ; chr2:206250975-206251174	Involved in guidance of NCC migration and restricting migratory paths of cranial and trunk NCCs, positioning sensory neurons and organizing their projections.	Gammill et al., 2007; Schwarz et al., 2008; Yu and Moens, 2005;
EPHB2	H	5.1251E-02	chr1:23164766-23164965 ; chr1:23164254-23164453 ; chr1:23162983-23163182 ; chr1:23162487-23162686	Ephrin B signaling is involved in targeting and restricting neural crest migration within branchial arches; compound EphB2/B3 knockout in mice leads to cleft palate.	Orioli et al., 1996; Risley et al., 2009; Smith et al., 1997;
BMP4	H	5.4181E-02	chr14:54911474-54911673 ; chr14:55093544-55093743; chr14:55094758-55094957 ; chr14:55095533-55095732	Proposed to be a crucial mediator of beak shape changes in Darwin's finches and of craniofacial shape and morphological adaptive radiation in Cichlid fish. CNCC-specific overexpression of BMP4 during mouse development results in the dramatic change of facial shape, with shortening in both the mandible and maxilla, rounding of the skull shape, and more anterior orientation of the eyes. In humans, mutations/variants in ***BMP4*** are associated with orofacial clefts, microphthalmia, and age of the primary tooth eruption.	Abzhanov et al., 2004; Albertson et al., 2005; Boell et al., 2013; Fatemifar et al., 2013; Tucker et al., 1998; Wu et al., 2004;
BMPER	C	2.2758E-05	chr7:33525807-33526006 ; chr7:33526320-33526519 ; chr7:33527256-33527455 ; chr7:33540319-33540518 ; chr7:33540928-33541127; (see Figure S4B)	Negative regulator of BMP4 function in osteoblast and chondrocyte differentiation (see also ***BMP4***). In humans, homozygous or heterozygous mutations in ***BMPER*** are associated with a skeletal disorder, diaphanospondylodysostosis, whose consistent craniofacial features include ocular hypertelorism, epicanthal folds, depressed nasal bridge with short nose, and low-set ears.	Binnerts et al., 2004; Funari et al., 2010; Moser et al., 2003;
PITX2	C	1.2564E-11	chr4:111230391-111230590; chr4:111230942-111231141 ; chr4:111820988-111821187	PITX2 haploinsufficiency is associated with Axenfeld-Rieger syndrome involving ocular anterior segment dysgenesis, tooth anomalies, and craniofacial anomalies such as maxillary hypoplasia with mid-face flattening and prominent forehead; in mice, ocular manifestations are largely recapitulated by the neural crest-specific knockout of Pitx2; genetically interacts with ***FOXC1***, see also ***FOXC1.***	Evans and Gage, 2005; Lu et al., 1999; Matt et al., 2005; Semina et al., 1996
FOXC1	C	3.4267E-02	chr6:1744897-1745096	Heterozygous mutations in ***FOXC1*** are associated with Axenfeld-Rieger syndrome (A-RS) involving ocular anterior segment dysgenesis, tooth anomalies, and maxillary and mandibular hypoplasia; dosage-dependent interactions with another A-RS gene ***PITX2*** have been observed; in mice, loss of FoxC1 results in bony syngnathia, defects in maxillary and mandibular structures, and agenesis of the temporomandibular joint; see also ***PITX2*** .	Berry et al., 2006; Inman et al., 2013; Kelberman et al., 2011; Mears et al., 1998; Tümer and Bach-Holm, 2009;
POU3F3	H	2.1354E-02	chr2:105024721-105024920 ; chr2:104990082-104990281 ; chr2:104989534-104989733 ; chr2:104937657-104937856	In mouse knockout leads to loss of squama temporalis and stapes fusion to styloid process.	Dheedene et al., 2014; Jeong et al., 2008;

(legend on next page)

expression for the bulk of the associated genes in the region (Figure 6E), suggesting that either (1) multiple genes in the vicinity must be under coordinated selection for these super-divergent regions to emerge or, more likely, that (2) strong selection on one or a few target genes could drive changes in the local enhancer landscape that have secondary effects on other genes in the vicinity. Altogether, we provide evidence that highly divergent clusters of tissue-specific enhancers may promote interspecies and intra-species phenotypic variation.

Resource for Studies of Human Morphological Evolution

In addition to informing the basic mechanisms underlying the *cis*-regulatory divergence of human and chimpanzee NC, our study also provides a rich resource for future investigations of morphological evolution of human craniofacial traits. Ontology annotations of all significantly species-biased enhancers reveal strong associations with processes important for various craniofacial structures that are diverging in human and chimps (Figure 7A). As examples, we highlight some of the most interesting divergent candidate genes in Figure 7B. These featured loci show species-biased expression in our RNA-seq and also map to regions with species-biased enhancer divergence and are emphasized due to their known associations with CNCC development and/or facial morphology. Nonetheless, it is important to bear in mind that the biases in gene expression and enhancer states highlighted in Figure 7 refer to the relative change between human and chimpanzee CNCCs, without ascribing the polarity of the change with respect to the ancestral status.

Our divergently expressed genes are known to be involved in multiple, distinct developmental processes that cooperate to influence differential allocation of CNCCs in facial primordia and, in turn, contribute to species-specific morphology (Fish et al., 2014). These processes (and associated species-biased genes) include: (1) CNCC specification (e.g., *PAX3*, *PAX7*), (2) migration and guidance of CNCC migratory paths (e.g., *EPHB2*, *NRP2*, *EDNRA*, *EDN3*), (3) modulation of CNCC proliferation at facial primordia (e.g., *BMP4*), and (4) regulation of CNCC differentiation (e.g., *PITX2*). Moreover, heterozygous mutations in many of these genes (e.g., *PAX3*, *PITX2*, *FOXC1*, *EDN3*, *BMPER*) are associated with human syndromes that include craniofacial manifestations, suggesting that altered gene dosage can drive both morphological variation between species and, below a certain threshold, disease-associated malformations (Figure 7B). Furthermore, many phenotypes of the highlighted genes affect aspects of head morphology that have diverged between humans and chimps (e.g., size of the mandible and maxilla, skull shape, and pigmentation) (Figure 7B and Discussion). Altogether, our study provides a wealth of candidate loci for further deep exploration in studies of human evolution and variation.

DISCUSSION

Our study utilizes primate cellular models to provide a comprehensive map of human and chimp regulatory divergence in a tissue with central relevance to the development of the head and face. We show that a common mechanism of regulatory divergence in higher primates is quantitative modulation of orthologous elements, driven largely through small numbers of sequence changes that perturb tissue-specific TF binding motifs. This is consistent with previous studies from closely related *Drosophila* or mouse species demonstrating that large effects can be conferred by a small number of mutations affecting direct and cooperative binding of key TFs (Bradley et al., 2010; He et al., 2011; Stefflova et al., 2013). Interestingly, we find that not all TF binding sites contribute equally to regulatory divergence—in fact, we identify a broad spectrum of regulatory motifs that vary in frequency and effect, suggesting a mechanism through which evolution can fine-tune *cis*-regulation across an enhancer landscape. One outlier in our analysis is the Coordinator motif, a de novo consensus sequence that is strongly predictive of the surrounding chromatin features and is highly enriched at species-biased enhancers. We speculate that the factor(s) that recognize the Coordinator motif play a privileged role in the establishment of enhancer competence in this cell context, reminiscent of the *Drosophila* TAGteam motif bound by a pioneer factor Zelda (Liang et al., 2008; Satija and Bradley, 2012). Furthermore, we find evidence of repressive inputs into quantitative modulation of enhancer activity, with a sizable number of motifs whose gain in strength negatively correlates with acquisition of permissive chromatin states.

Our work provides a rich framework for future gene-centric studies on the developmental mechanisms of human morphological evolution. Indeed, our approach identified loci that are known to profoundly affect NC development and craniofacial morphology, often in a dosage-sensitive manner. For example, we observed that two genes involved in CNCC specification, *PAX3* and *PAX7*, are expressed at higher levels in chimps and are associated with clusters of chimp-biased enhancers. In mice, mutations of these TFs lead to reduction of pigmentation and snout length (*Pax3*) (Tremblay et al., 1995) and reduction of maxilla and pointed snout (*Pax7*) (Mansouri et al., 1996), features that are consistent with smaller jaw size and hypopigmentation of humans as compared to chimps. Furthermore, humans are sensitive to alterations of *PAX3* dosage, as haploinsufficiency of this gene is associated with craniofacial, auditory, and pigmentation defects (Waardenburg syndrome, OMIM #193510), and genetic variants at this locus have been identified in GWAS studies as regulators of normal-range facial shape (Liu et al., 2012; Paternoster et al., 2012). Thus, variation in

Figure 7. Species-Biased Enhancers Are Associated with Genes Affecting Craniofacial Structures

(A) GREAT term enrichments and associated facial regions indicated for human-biased enhancers ($q < 0.01$, baseMean > 300) and chimp-biased enhancers ($q < 0.01$, baseMean > 300); binomial raw p values are shown below. Ontology categories are color coded (human phenotypes, red; mouse phenotypes, blue; biological processes, green).

(B) Table of highlighted divergently expressed genes showing direction of bias (human-biased versus chimp-biased indicated by H or C, respectively), DESeq adjusted p value of expression divergence, coordinates of nearby species-biased enhancers with corresponding bias (hg19), description of genetic phenotypes, disease associations, comments, and relevant references. Full reference information can be found in Table S1.

PAX3 and PAX7 levels represents an attractive possible mechanism for mediating facial shape divergence between humans and chimpanzees.

We also find evidence that genes already known to affect facial morphology in other species, such as *BMP4*, are diverging in higher primates as well. BMP4 is the most well-understood example of a factor that influenced craniofacial morphological change during evolution, as it has been implicated in mediating changes in beak morphology in Darwin's finches (Abzhanov et al., 2004) and in jaw shape in Cichlid fish (Albertson et al., 2005). We were therefore intrigued to note that *BMP4* is associated with strongly human-biased enhancers and is expressed at higher levels in humans than in chimps. Conversely, expression of the BMP4 inhibitor *BMPER* was significantly chimp biased and showed dramatic strengthening of the local chimp enhancer landscape. What would be the potential effects of elevated BMP4 expression on primate facial development? Interestingly, in the mouse, CNCC-specific overexpression of *BMP4* results in a dramatic change of facial shape, with shortening of both the mandible and maxilla, rounding of the skull, and more anterior orientation of the eyes (Bonilla-Claudio et al., 2012)—morphological changes that resemble those observed between human and chimps. Thus, the same molecular mechanism that has been postulated to influence beak morphology in Darwin's finches may also contribute to our uniquely human facial features.

Even more intriguing, of five chromosomal regions that have been associated with normal-range human facial variation in GWAS, three (*PRDM16*, *COL17A1*, and *PAX3*) coincide with clusters of species-biased enhancers uncovered in our study (Liu et al., 2012; Paternoster et al., 2012), suggesting a significant overlap between loci regulating intra- and inter-species variation of facial shape in higher primates. We therefore hypothesize that other divergent clusters identified in our study represent novel candidates for loci involved in the regulation of facial shape in humans. More broadly, we suggest that comparisons of human regulatory landscapes with those of a closely related primate in any tissue of interest may provide an effective strategy to identify candidate loci involved in normal-range and disease-associated variation.

EXPERIMENTAL PROCEDURES

CNCC Derivation

Pluripotent lines were differentiated into CNCC as previously described (Rada-Iglesias et al., 2012). Details are provided in the Supplemental Experimental Procedures.

Chromatin Immunoprecipitation and Preparation of ChIP-Seq Libraries

Chromatin immunoprecipitation (ChIP) was performed using ~0.5–1 × 10^7 CNCCs per experiment, as previously described (Bajpai et al., 2010; Rada-Iglesias et al., 2011, 2012). Antibodies used for ChIPs are listed in the Supplemental Experimental Procedures. Sequencing libraries were prepared starting from 30 ng of ChIP DNA using the NEBNext Multiplex Oligos for Illumina kit (Cat# E7335S). Libraries were multiplexed four to six samples per lane for 1 × 50 bp next-gen sequencing on Illumina HiSeq platform.

Quantitative Analysis of H3K27ac ChIP-Seq and Identification of Divergence

All sequencing reads were aligned to both reference genomes (hg19 and panTro3) using default settings with bowtie2.2.4, regardless of species of origin. Modal peak positions for candidate regulatory elements were determined using a mean shift procedure, described in the Supplemental Experimental Procedures. To obtain count statistics for each H3K27ac ChIP alignment, we counted read coverage in a 1.6 kb window surrounding modal peak positions. ENCODE-blacklisted regions and outlier regions with high counts in control input sequences relative to ChIP were removed as artifacts. Scores for visualization and classification of remaining ChIPs were obtained using a kernel density estimate, as previously described (Buecker et al., 2014).

Calculations of species bias were inferred with DESeq2, based on the read counts from all replicates of H3K27ac at candidate enhancers from three human lines (one hESC, two iPSC) and two chimp lines (two iPSC). DESeq2 analysis was performed separately for panTro3 and hg19 counts; then conservatively, the higher p-adj value and lower abs(log2FoldChange) of the analysis from either hg19 or panTro3 were assigned to each region, while rare regions with discordant calls were excluded from list of biased sites (less than 0.1%).

ACCESSION NUMBERS

All sequencing data sets were deposited in the NCBI GEO repository under accession ID GEO: GSE70751.

SUPPLEMENTAL INFORMATION

Supplemental Information includes Supplemental Experimental Procedures, seven figures, and three tables and can be found with this article online at http://dx.doi.org/10.1016/j.cell.2015.08.036.

ACKNOWLEDGMENTS

We thank D. Kingsley, R. Greenberg, J. Buenrostro, and Wysocka lab members for comments on the manuscript. We also thank R. Aho and J.D. Benazet for help with imaging of mouse transgenic embryos and interpretation of staining patterns, as well as P. Nano and E. Grow for help generating reporter reagents. This work was supported by W.M. Keck Foundation, Stanford School of Medicine Innovation Fund, and NIH R01 GM095555 (J.W.) and U01 DE024430 (J.W. and L.S.), as well as CIRM training grant (TG2-01159) (S.L.P.). This work was also partially supported by funds from NIH TR01 MH095741, the Helmsley Charitable Fund, the Mathers Foundation, and the JPB Foundation (F.H.G.).

Received: February 3, 2015
Revised: May 6, 2015
Accepted: July 21, 2015
Published: September 10, 2015

REFERENCES

Abzhanov, A., Protas, M., Grant, B.R., Grant, P.R., and Tabin, C.J. (2004). Bmp4 and morphological variation of beaks in Darwin's finches. Science *305*, 1462–1465.

Albertson, R.C., Streelman, J.T., Kocher, T.D., and Yelick, P.C. (2005). Integration and evolution of the cichlid mandible: the molecular basis of alternate feeding strategies. Proc. Natl. Acad. Sci. USA *102*, 16287–16292.

Attanasio, C., Nord, A.S., Zhu, Y., Blow, M.J., Li, Z., Liberton, D.K., Morrison, H., Plajzer-Frick, I., Holt, A., Hosseini, R., et al. (2013). Fine tuning of craniofacial morphology by distant-acting enhancers. Science *342*, 1241006.

Bajpai, R., Chen, D.A., Rada-Iglesias, A., Zhang, J., Xiong, Y., Helms, J., Chang, C.-P., Zhao, Y., Swigut, T., and Wysocka, J. (2010). CHD7 cooperates with PBAF to control multipotent neural crest formation. Nature *463*, 958–962.

Bilsborough, A., and Wood, B.A. (1988). Cranial morphometry of early hominids: facial region. Am. J. Phys. Anthropol. *76*, 61–86.

Bonilla-Claudio, M., Wang, J., Bai, Y., Klysik, E., Selever, J., and Martin, J.F. (2012). Bmp signaling regulates a dose-dependent transcriptional program to control facial skeletal development. Development *139*, 709–719.

Bradley, R.K., Li, X.-Y., Trapnell, C., Davidson, S., Pachter, L., Chu, H.C., Tonkin, L.A., Biggin, M.D., and Eisen, M.B. (2010). Binding site turnover produces pervasive quantitative changes in transcription factor binding between closely related Drosophila species. PLoS Biol. *8*, e1000343.

Bronner, M.E., and LeDouarin, N.M. (2012). Development and evolution of the neural crest: an overview. Dev. Biol. *366*, 2–9.

Buecker, C., Srinivasan, R., Wu, Z., Calo, E., Acampora, D., Faial, T., Simeone, A., Tan, M., Swigut, T., and Wysocka, J. (2014). Reorganization of enhancer patterns in transition from naive to primed pluripotency. Cell Stem Cell *14*, 838–853.

Buenrostro, J.D., Giresi, P.G., Zaba, L.C., Chang, H.Y., and Greenleaf, W.J. (2013). Transposition of native chromatin for fast and sensitive epigenomic profiling of open chromatin, DNA-binding proteins and nucleosome position. Nat. Methods *10*, 1213–1218.

Cain, C.E., Blekhman, R., Marioni, J.C., and Gilad, Y. (2011). Gene expression differences among primates are associated with changes in a histone epigenetic modification. Genetics *187*, 1225–1234.

Carroll, S.B. (2008). Evo-devo and an expanding evolutionary synthesis: a genetic theory of morphological evolution. Cell *134*, 25–36.

Cordaux, R., and Batzer, M.A. (2009). The impact of retrotransposons on human genome evolution. Nat. Rev. Genet. *10*, 691–703.

Cordero, D.R., Brugmann, S., Chu, Y., Bajpai, R., Jame, M., and Helms, J.A. (2011). Cranial neural crest cells on the move: their roles in craniofacial development. Am. J. Med. Genet. A. *155A*, 270–279.

Cotney, J., Leng, J., Yin, J., Reilly, S.K., DeMare, L.E., Emera, D., Ayoub, A.E., Rakic, P., and Noonan, J.P. (2013). The evolution of lineage-specific regulatory activities in the human embryonic limb. Cell *154*, 185–196.

Creyghton, M.P., Cheng, A.W., Welstead, G.G., Kooistra, T., Carey, B.W., Steine, E.J., Hanna, J., Lodato, M.A., Frampton, G.M., Sharp, P.A., et al. (2010). Histone H3K27ac separates active from poised enhancers and predicts developmental state. Proc. Natl. Acad. Sci. USA *107*, 21931–21936.

Fish, J.L., Sklar, R.S., Woronowicz, K.C., and Schneider, R.A. (2014). Multiple developmental mechanisms regulate species-specific jaw size. Development *141*, 674–684.

Gompel, N., Prud'homme, B., Wittkopp, P.J., Kassner, V.A., and Carroll, S.B. (2005). Chance caught on the wing: cis-regulatory evolution and the origin of pigment patterns in Drosophila. Nature *433*, 481–487.

Gronau, I., Arbiza, L., Mohammed, J., and Siepel, A. (2013). Inference of natural selection from interspersed genomic elements based on polymorphism and divergence. Mol. Biol. Evol. *30*, 1159–1171.

He, Q., Bardet, A.F., Patton, B., Purvis, J., Johnston, J., Paulson, A., Gogol, M., Stark, A., and Zeitlinger, J. (2011). High conservation of transcription factor binding and evidence for combinatorial regulation across six Drosophila species. Nat. Genet. *43*, 414–420.

Heintzman, N.D., Stuart, R.K., Hon, G., Fu, Y., Ching, C.W., Hawkins, R.D., Barrera, L.O., Van Calcar, S., Qu, C., Ching, K.A., et al. (2007). Distinct and predictive chromatin signatures of transcriptional promoters and enhancers in the human genome. Nat. Genet. *39*, 311–318.

Hong, J.-W., Hendrix, D.A., and Levine, M.S. (2008). Shadow enhancers as a source of evolutionary novelty. Science *321*, 1314.

Hubisz, M.J., and Pollard, K.S. (2014). Exploring the genesis and functions of Human Accelerated Regions sheds light on their role in human evolution. Curr. Opin. Genet. Dev. *29*, 15–21.

Jheon, A.H., and Schneider, R.A. (2009). The cells that fill the bill: neural crest and the evolution of craniofacial development. J. Dent. Res. *88*, 12–21.

Kaessmann, H., Wiebe, V., and Pääbo, S. (1999). Extensive nuclear DNA sequence diversity among chimpanzees. Science *286*, 1159–1162.

King, M.C., and Wilson, A.C. (1975). Evolution at two levels in humans and chimpanzees. Science *188*, 107–116.

Liang, H.-L., Nien, C.-Y., Liu, H.-Y., Metzstein, M.M., Kirov, N., and Rushlow, C. (2008). The zinc-finger protein Zelda is a key activator of the early zygotic genome in Drosophila. Nature *456*, 400–403.

Lieberman, D.E. (1998). Sphenoid shortening and the evolution of modern human cranial shape. Nature *393*, 158–162.

Liu, F., van der Lijn, F., Schurmann, C., Zhu, G., Chakravarty, M.M., Hysi, P.G., Wollstein, A., Lao, O., de Bruijne, M., Ikram, M.A., et al. (2012). A genome-wide association study identifies five loci influencing facial morphology in Europeans. PLoS Genet. *8*, e1002932.

Mansouri, A., Stoykova, A., Torres, M., and Gruss, P. (1996). Dysgenesis of cephalic neural crest derivatives in Pax7-/- mutant mice. Development *122*, 831–838.

Marchetto, M.C.N., Narvaiza, I., Denli, A.M., Benner, C., Lazzarini, T.A., Nathanson, J.L., Paquola, A.C.M., Desai, K.N., Herai, R.H., Weitzman, M.D., et al. (2013). Differential L1 regulation in pluripotent stem cells of humans and apes. Nature *503*, 525–529.

McLean, C.Y., Reno, P.L., Pollen, A.A., Bassan, A.I., Capellini, T.D., Guenther, C., Indjeian, V.B., Lim, X., Menke, D.B., Schaar, B.T., et al. (2011). Human-specific loss of regulatory DNA and the evolution of human-specific traits. Nature *471*, 216–219.

Odom, D.T., Dowell, R.D., Jacobsen, E.S., Gordon, W., Danford, T.W., MacIsaac, K.D., Rolfe, P.A., Conboy, C.M., Gifford, D.K., and Fraenkel, E. (2007). Tissue-specific transcriptional regulation has diverged significantly between human and mouse. Nat. Genet. *39*, 730–732.

Paternoster, L., Zhurov, A.I., Toma, A.M., Kemp, J.P., St Pourcain, B., Timpson, N.J., McMahon, G., McArdle, W., Ring, S.M., Smith, G.D., et al. (2012). Genome-wide association study of three-dimensional facial morphology identifies a variant in PAX3 associated with nasion position. Am. J. Hum. Genet. *90*, 478–485.

Pollard, K.S., Salama, S.R., Lambert, N., Lambot, M.-A., Coppens, S., Pedersen, J.S., Katzman, S., King, B., Onodera, C., Siepel, A., et al. (2006). An RNA gene expressed during cortical development evolved rapidly in humans. Nature *443*, 167–172.

Prabhakar, S., Poulin, F., Shoukry, M., Afzal, V., Rubin, E.M., Couronne, O., and Pennacchio, L.A. (2006). Close sequence comparisons are sufficient to identify human cis-regulatory elements. Genome Res. *16*, 855–863.

Prabhakar, S., Visel, A., Akiyama, J.A., Shoukry, M., Lewis, K.D., Holt, A., Plajzer-Frick, I., Morrison, H., Fitzpatrick, D.R., Afzal, V., et al. (2008). Human-specific gain of function in a developmental enhancer. Science *321*, 1346–1350.

Rada-Iglesias, A., Bajpai, R., Swigut, T., Brugmann, S.A., Flynn, R.A., and Wysocka, J. (2011). A unique chromatin signature uncovers early developmental enhancers in humans. Nature *470*, 279–283.

Rada-Iglesias, A., Bajpai, R., Prescott, S., Brugmann, S.A., Swigut, T., and Wysocka, J. (2012). Epigenomic annotation of enhancers predicts transcriptional regulators of human neural crest. Cell Stem Cell *11*, 633–648.

Satija, R., and Bradley, R.K. (2012). The TAGteam motif facilitates binding of 21 sequence-specific transcription factors in the Drosophila embryo. Genome Res. *22*, 656–665.

Schmidt, D., Wilson, M.D., Ballester, B., Schwalie, P.C., Brown, G.D., Marshall, A., Kutter, C., Watt, S., Martinez-Jimenez, C.P., Mackay, S., et al. (2010). Five-vertebrate ChIP-seq reveals the evolutionary dynamics of transcription factor binding. Science *328*, 1036–1040.

Shapiro, M.D., Marks, M.E., Peichel, C.L., Blackman, B.K., Nereng, K.S., Jónsson, B., Schluter, D., and Kingsley, D.M. (2004). Genetic and developmental basis of evolutionary pelvic reduction in threespine sticklebacks. Nature *428*, 717–723.

Shibata, Y., Sheffield, N.C., Fedrigo, O., Babbitt, C.C., Wortham, M., Tewari, A.K., London, D., Song, L., Lee, B.-K., Iyer, V.R., et al. (2012). Extensive evolutionary changes in regulatory element activity during human origins are associated with altered gene expression and positive selection. PLoS Genet. *8*, e1002789.

Spoor, F., Wood, B., and Zonneveld, F. (1994). Implications of early hominid labyrinthine morphology for evolution of human bipedal locomotion. Nature *369*, 645–648.

Stefflova, K., Thybert, D., Wilson, M.D., Streeter, I., Aleksic, J., Karagianni, P., Brazma, A., Adams, D.J., Talianidis, I., Marioni, J.C., et al. (2013). Cooperativity

and rapid evolution of cobound transcription factors in closely related mammals. Cell *154*, 530–540.

Tremblay, P., Kessel, M., and Gruss, P. (1995). A transgenic neuroanatomical marker identifies cranial neural crest deficiencies associated with the Pax3 mutant Splotch. Dev. Biol. *171*, 317–329.

Twigg, S.R.F., Versnel, S.L., Nürnberg, G., Lees, M.M., Bhat, M., Hammond, P., Hennekam, R.C.M., Hoogeboom, A.J.M., Hurst, J.A., Johnson, D., et al. (2009). Frontorhiny, a distinctive presentation of frontonasal dysplasia caused by recessive mutations in the ALX3 homeobox gene. Am. J. Hum. Genet. *84*, 698–705.

Vierstra, J., Rynes, E., Sandstrom, R., Zhang, M., Canfield, T., Hansen, R.S., Stehling-Sun, S., Sabo, P.J., Byron, R., Humbert, R., et al. (2014). Mouse regulatory DNA landscapes reveal global principles of cis-regulatory evolution. Science *346*, 1007–1012.

Villar, D., Berthelot, C., Aldridge, S., Rayner, T.F., Lukk, M., Pignatelli, M., Park, T.J., Deaville, R., Erichsen, J.T., Jasinska, A.J., et al. (2015). Enhancer evolution across 20 mammalian species. Cell *160*, 554–566.

Visel, A., Minovitsky, S., Dubchak, I., and Pennacchio, L.A. (2007). VISTA Enhancer Browser–a database of tissue-specific human enhancers. Nucleic Acids Res. *35*, D88–D92.

Whyte, W.A., Orlando, D.A., Hnisz, D., Abraham, B.J., Lin, C.Y., Kagey, M.H., Rahl, P.B., Lee, T.I., and Young, R.A. (2013). Master transcription factors and mediator establish super-enhancers at key cell identity genes. Cell *153*, 307–319.

Wong, E.S., Thybert, D., Schmitt, B.M., Stefflova, K., Odom, D.T., and Flicek, P. (2014). Decoupling of evolutionary changes in transcription factor binding and gene expression in mammals. Genome Res.

Wray, G.A. (2007). The evolutionary significance of cis-regulatory mutations. Nat. Rev. Genet. *8*, 206–216.

Zhou, X., Cain, C.E., Myrthil, M., Lewellen, N., Michelini, K., Davenport, E.R., Stephens, M., Pritchard, J.K., and Gilad, Y. (2014). Epigenetic modifications are associated with inter-species gene expression variation in primates. Genome Biol. *15*, 547.

Cell

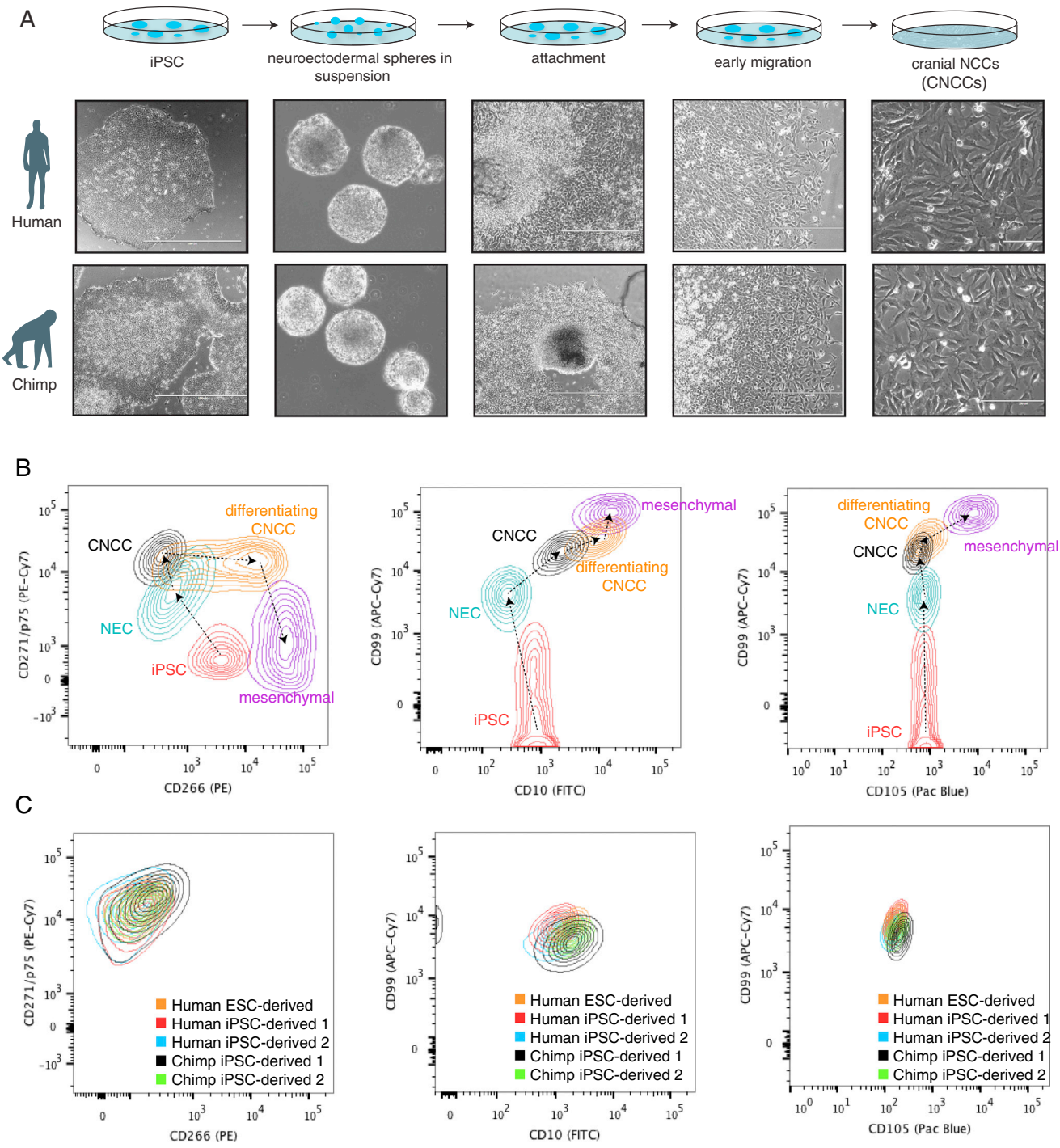

Figure S1. Developmental Staging and Cellular Heterogeneity in the In-Vitro-Derived Human and Chimp CNCCs, Related to Figure 1

(A) Brightfield images of steps in derivation of human and chimp CNCCs. CNCCs are differentiated from iPSCs, first forming neuroectodermal spheres which then later attach and give rise to migratory CNCCs which can be maintained up to 18 passages.

(B) Plots showing dynamic changes in surface "cluster of differentiation" (CD) markers: CD10, CD99, CD105, CD266, and CD271 (p75) over the course of the in vitro derivation of neural crest cells from iPSCs, as well as further differentiation past the neural crest state to mesenchymal lineages.

(**C**) Analysis of surface marker expression at passage 4 CNCCs isolated from a hESC line (H9s), two human iPSC lines and two chimp iPSC lines showing > 90% homogeneity in representative replicates from each genetic background. Contour lines represent 90% of counted cells.

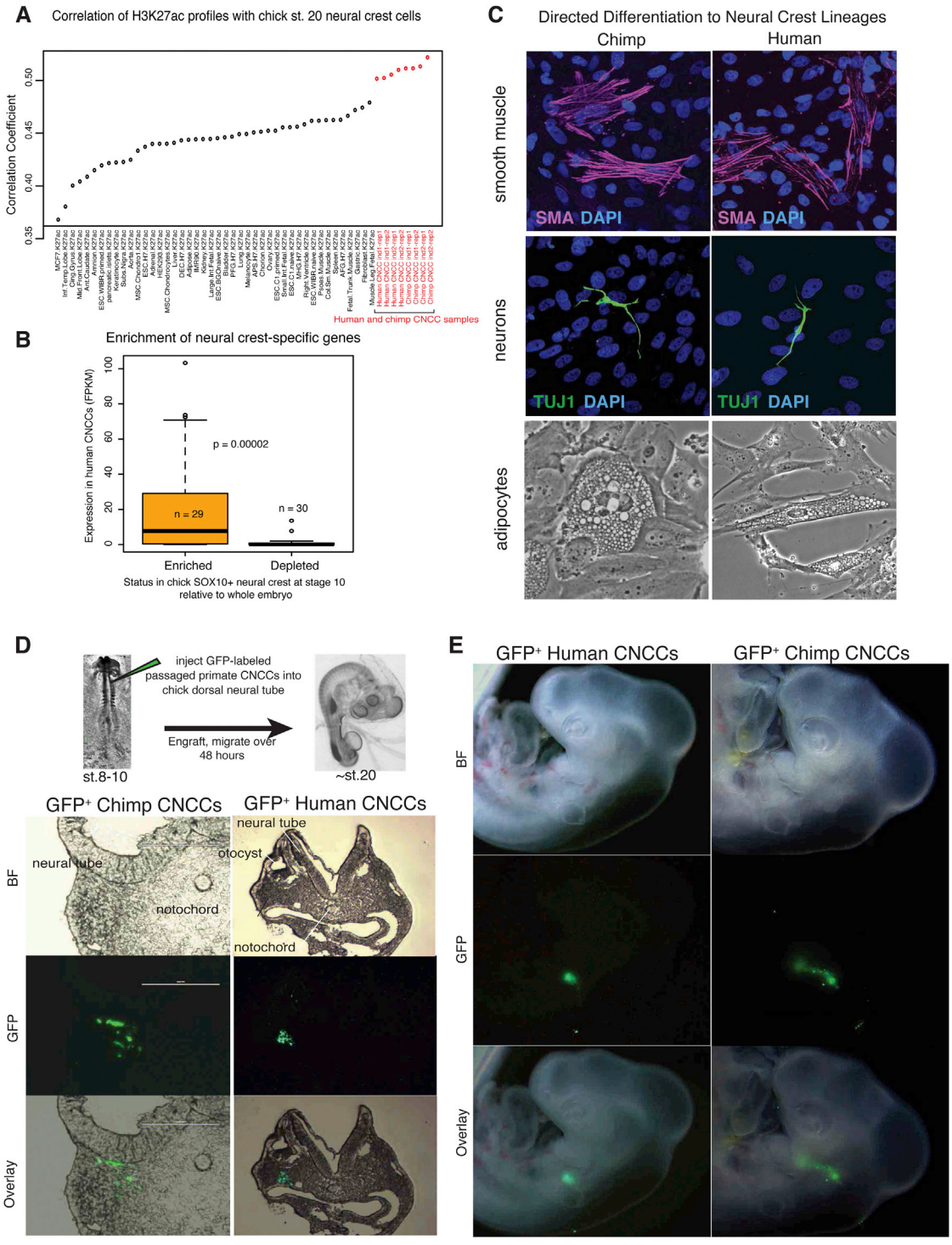

Figure S2. Characterization of In-Vitro-Derived Human and Chimp CNCCs, Related to Figure 1

(A) Correlation coefficient of global H3K27ac profiles from post-migratory CNCCs populating the frontonasal prominence of chick embryo at Hamburger-Hamilton st.20 compared with human in vitro-derived CNCC H3K27ac profiles and with 44 other human cell types.

(B) Average expression level (FPKM) in human CNCCs of transcripts described in Simões-Costa et al., 2014 as the most neural crest-enriched versus neural crest depleted, as defined by transcriptome analysis of sorted SOX10+ migratory neural crest cells isolated from chick embryos. Central bar represents the median, box outline represents first and third quartile, and whiskers extend to furthest datapoint within 1.5× box length way from the box.

(legend continued on next page)

(C) CNCCs at p4 from both species were further differentiated under defined conditions to smooth muscle cells, neurons and adipocytes, then imaged by confocal microscopy. Smooth muscle actin (SMA) is shown in red, neuron-specific class III beta-tubulin (TUJ1) is shown in green, overlaid with DAPI-stained nuclei, and vacuolated adipocytes are shown by brightfield at the bottom.

(D and E) In vitro-derived GFP-labeled human and chimp CNCCs (p4) were injected into the dorsal neural tube of st.8-10 chick embryos, then cultured for 48 hr and imaged for incorporation of GFP^+ cells. Sections showing engraftment into facial structures in (D) and whole mount images showing migration into branchial arches in (E).

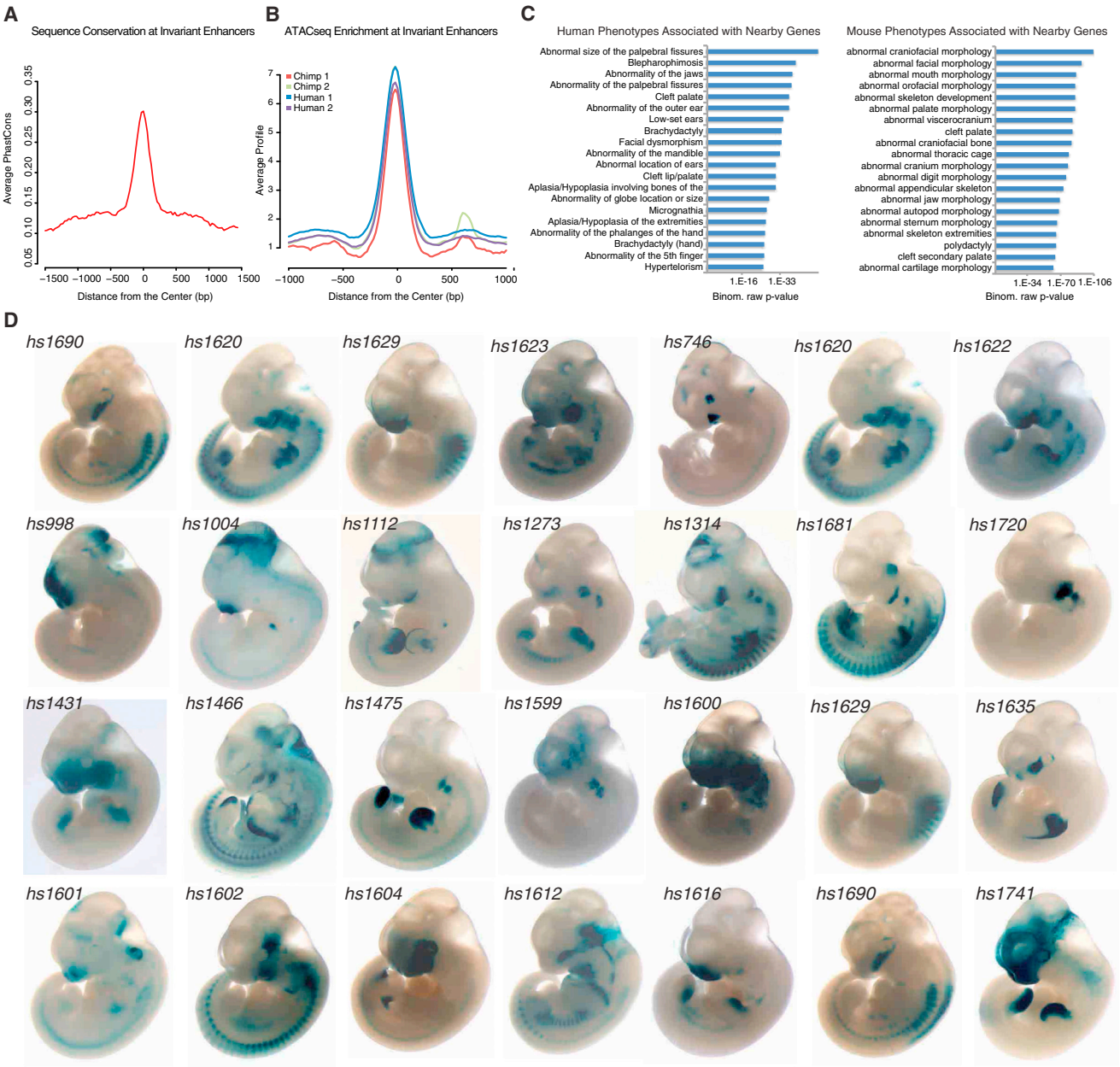

Figure S3. Conservation Signatures, Chromatin Accessibility, Gene Association, and VISTA Database Overlap for Enhancer Candidates Identified through Epigenomic Mapping, Related to Figure 1

(A) Average PhastCons score for 1.5kb region surrounding the center of epigenetically-marked elements classified as enhancers (without species-bias, p-value > 0.95) that were mapped to hg19.

(B) Average ATAC-seq enrichment for 1kb region surrounding the center of epigenomically-marked elements classified as enhancers (without species-bias, p- value > 0.95) that were mapped to hg19.

(C) Human and mouse phenotype term enrichments from GREAT for genes near epigenomically-marked elements classified as enhancers (without species-bias, p-value > 0.95) that were mapped to hg19.

(D) Representative *lacZ* stains of regulatory regions overlapping active human CNCC enhancers that were tested in mouse transgenesis assays by the VISTA enhancer database (Visel et al., 2007).

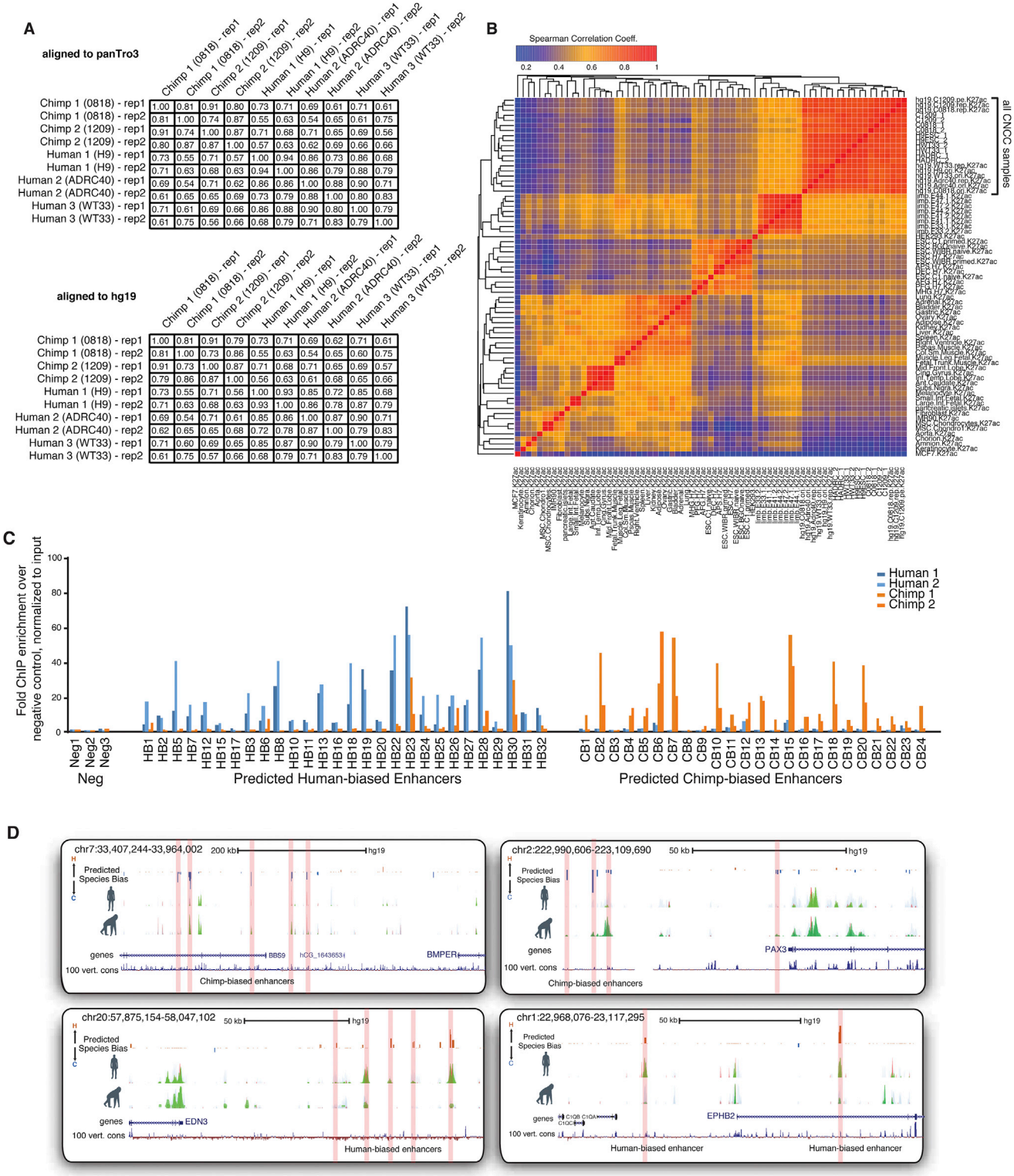

Figure S4. Genome-wide Comparisons of Epigenomic Patterns in Human and Chimp CNCCs, ChIP-qPCR Validation, and Examples of Species-Biased Enhancers, Related to Figure 2

(A) Spearman correlation coefficient for H3K27ac enrichments at top ~75K candidate enhancer regions from all human cell lines (H9, WT33, ADRC40) and chimp cell lines (0818, 1209) mapped to hg19 (bottom) or panTro3 (top) in biological replicate.

(legend continued on next page)

(B) Clustering of 45 public and 19 CNCC datasets based on H3K27ac enrichments at the 50000 most significant regulatory elements shared between combined CNCC mapped regulatory regions and ENCODE regions inferred from ENCODE TF ChIPs + DNase HS downloaded from UCSC genome browser.
(C) H3K27ac ChIP-qPCR from independent CNCC differentiations at p4 for two human and two chimp genetic backgrounds using primers targeting 28 human-biased enhancers ($q < 0.001$), 24 chimp-biased enhancers ($q < 0.001$), and 3 negative control regions. ChIP enrichment was normalized to input, and represented as fold enrichment relative to Neg1 region.
(D) Genome browser tracks showing overlay of H3K27 (green), p300 (red) and H3K4me1 (blue) near *BMPER* (chr7:33,407,244-33,964,002, top left), *PAX3* (chr2:222,990,606 - 223,109,690, top right), *EDN3* (chr20:57,875,154 - 58,047,102) and *EPHB2* (chr1:22,968,076 - 23,117,295). The predicted species-bias is shown above, with human-bias shown in bronze and chimp-bias shown in indigo. Conservation track shown below. For all profiles, hg19 is used as reference genome.

A

Enhancer of Interest	Pronuclei Injected	Embryos	Survival	PCR+	Transgenesis	LacZ+	LacZ+ / PCR+
CNTNAP2x3-Human	**187**	**58**	31.02%	**6**	3.21%	**5**	83.33%
CNTNAP2x3-Chimp	**447**	**145**	32.44%	**11**	2.46%	**5**	45.45%
PAPPAx3-Human	**363**	**139**	38.29%	**9**	2.48%	**7**	77.78%
PAPPAx3-Chimp	**448**	**125**	27.90%	**19**	4.24%	**11**	57.89%

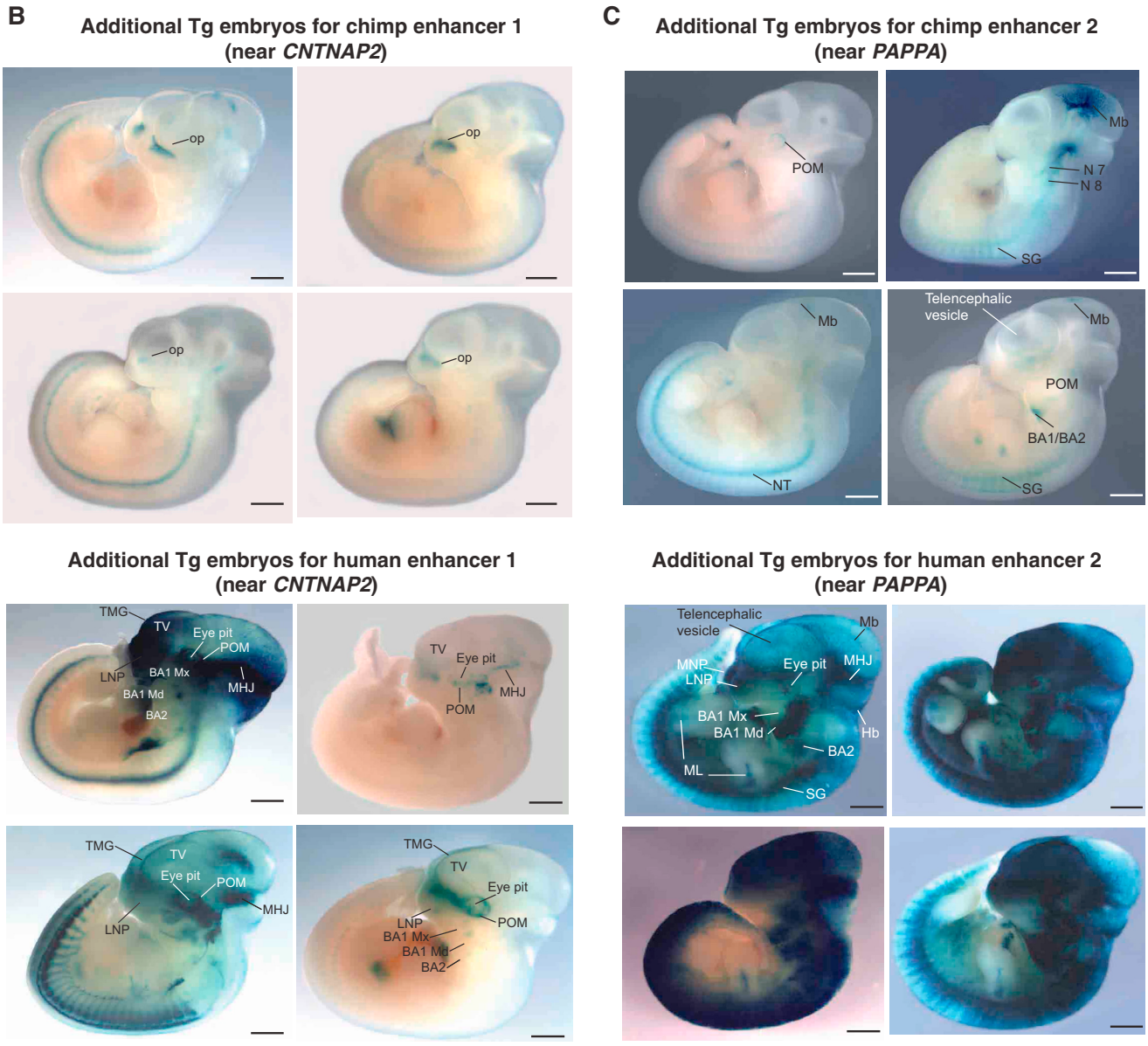

Figure S5. Additional *lacZ* Stains of *CNTNAP2* and *PAPPA* Enhancers Tested in Mouse Transgenesis Assays, Related to Figure 3

(A) Summary of transgenic analysis. Table showing number of pronuclei injected, number of surviving embryos after injection, number and percentage of those that tested positive by PCR for reporter integration, number of embryos with detectable *LacZ* expression after staining, and the percentage of lacZ-positive embryos over the total number of PCR-positive transgenic mice recovered per construct. Error bars represent approximate SE.

(B) Analysis of enhancer activity for chimpanzee and human enhancer 1 (near *CNTNAP2)* in a *lacZ* reporter transgenic mouse assay reveals gain of expression domains for the human enhancer. Embryos obtained from independent transgene integrations are shown for the chimpanzee and the human Enhancer 1, respectively (upper panels, chimpanzee; lower panels, human; see also embryos in Figure 3). In addition to expression in the olfactory placode (op) and its

(legend continued on next page)

projections detected for the chimpanzee enhancer, the human enhancer exhibits reproducible activity in newly acquired expression domains that are present in at least 3 independent embryos: telencephalic vesicles (TV); telencephalic midline groove (TMG); eye pit; periocular mesenchyme (POM); lateral and medial nasal processes (MNP and LNP); midbrain/hindbrain junction (MHJ); patches within maxillary (Mx) and mandibular (Md) processes of branchial arch 1 (BA1) and BA2. Scale bars: 100 μm.

(C) Analysis of enhancer activity for chimpanzee and human e 2 (near *PAPPA*) in a *lacZ* reporter transgenic mouse assay reveals gain of expression domains for the human enhancer. Embryos obtained from independent transgene integrations are shown for the chimpanzee and the human e 2, respectively (upper panels, chimpanzee; lower panels, human; see also embryos in Figure 3 E-H). The chimpanzee enhancer shows reproducible expression in craniofacial nerve (N) domains (N 7 and N 8); midbrain (Mb); neural tube (NT); periocular mesenchyme (POM); and sympathetic ganglia (SG). In addition to the expression patterns shared with the chimpanzee enhancer, the human enhancer exhibits reproducible strong activity in newly acquired domains (present in 7 independent embryos, of which representative ones are shown): telencephalic vesicles; eye pit; lateral and medial nasal processes (MNP and LNP); midbrain/hindbrain junction (MHJ); hindbrain (Hb); proximal maxillary (Mx) and mandibular (Md) processes of branchial arch 1 (BA1) and BA2. Scale bars: 100 μm.

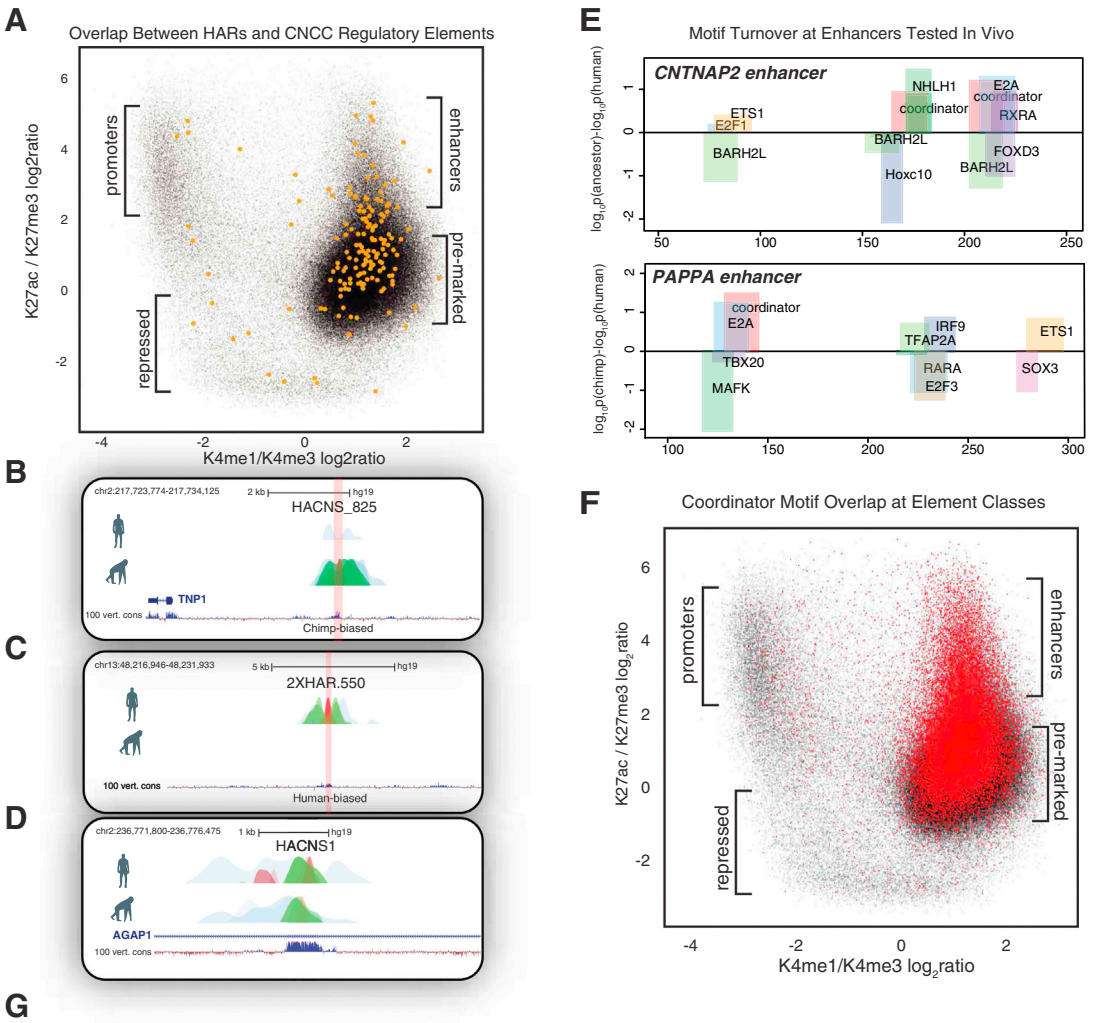

(legend on next page)

Figure S6. Human Accelerated Regions Overlapping CNCC Enhancers, Coordinator Motif Enrichments at Distal Enhancers, and Comparisons with Hominin Outgroups, Related to Figure 4

(A) Scatterplot of the log ratio of H3K4me1 / H3K4me3 (x axis) relative to ratio of H3K27ac / H3K27me3 (y axis) split genomic elements into four classes based on chromatin status: promoters, enhancers, repressed and pre-marked/pioneered sites. Regulatory elements overlapping with human accelerated regions (HARs), indicated by colored points.

(B–D) Genome browser tracks showing overlay of H3K27 (green), p300 (red) and H3K4me1 (blue) near (A) HACNS_825 (chimp-biased, q-value = 2.86E-18), (B) 2xHAR.550 (human-biased, q = 8.66823E-4) and (C) HACSN1/HAR2 (q-value = 0.339). All shown in hg19.

(E) Turnover of recognizable transcription factor motifs within the enhancer 1 (near *CNTNAP2*) and enhancer 2 (near *PAPPA*) between humans and chimps. Changes in the match to the motif consensus across assemblies are represented as at $\log_{10}p_{chimp}$ - at $\log_{10}p_{human}$. Of note, mutations within enhancer 1 were entirely human-derived relative to the human-chimp ancestor (so, in this context $\log_{10}p_{ancestor} = \log_{10}p_{chimp)}$. Both enhancers show gains in human genome for activating motifs (eg, Coordinator, RXRA, TFAP2A, ETS1) and/or loss of repressive motifs (eg, HOXC1).

(F) Coordinator motif is enriched at chromatin sites with enhancer like markings ($p < <10^{-16}$, Fisher's exact test). Scatterplots of the log ratio of H3K4me1 / H3K4me3 (x axis) relative to ratio of H3K27ac / H3K27me3 (y axis) split chromatin into four classes: promoters, enhancers, repressed and pre-marked/pioneered sites. Elements containing Coordinator motif at fimo p-value cutoff < 0.0001 are shown in red.

(G) Comparison of sequence changes within the Coordinator motif (-log10p-value of fit to the consensus) between the human-chimp ancestor (above) or modern humans (below) with Neanderthal and Denisovan ancestral outgroups. Ancestral sequences corresponding to CNCC enhancers were constructed using the Ensembl EPO pipeline, and corresponding Neanderthal and Denisovan sequences were extracted from published assemblies (Meyer et al.,. 2012; Prüfer et al., 2014). Data points were jittered to allow better visualization. Schematics of how the distribution reflects gains versus losses in a particular lineage are shown on the far left.

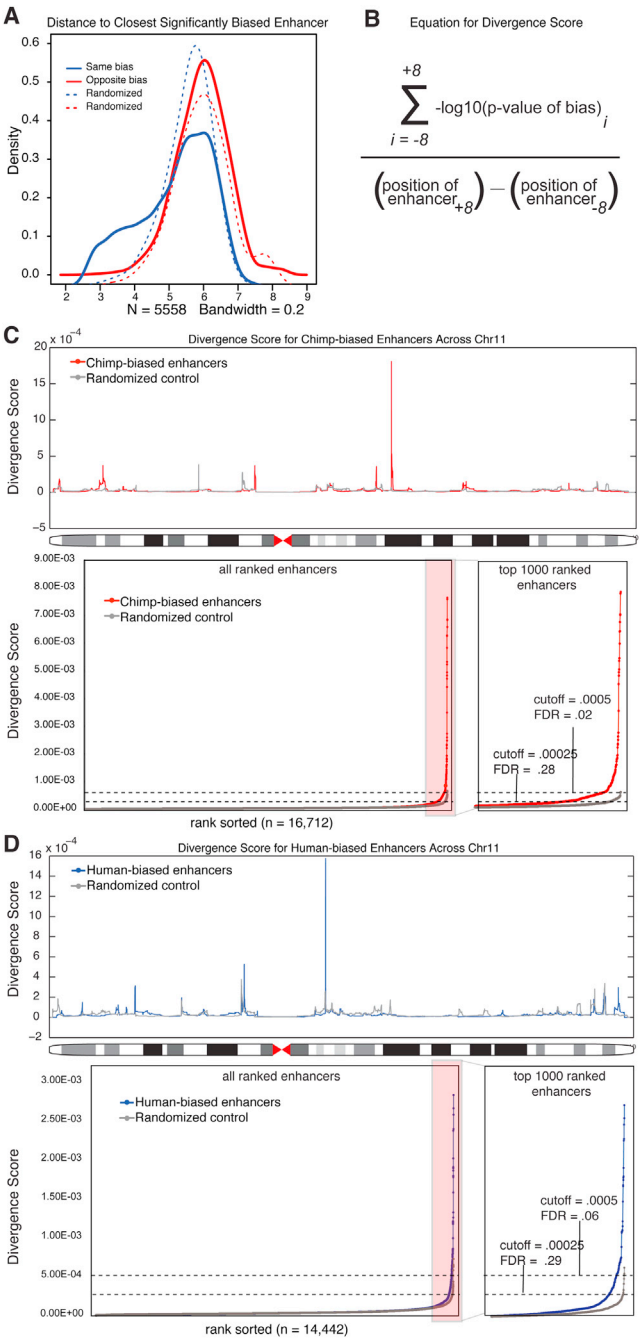

Figure S7. Identification of Clusters of Regulatory Divergence, Related to Figure 6

(A) Distribution of distances of regulatory region with significant change between the species to another such region with the direction of bias (blue) or opposite bias (red). As a control, the same calculation was performed on two sets of intervals with shuffled bias direction (dotted lines).

(B) Calculation of divergence score for sorted enhancers (enhancer index = i).

(C and D) Ideogram on chr11 (top) and genome-wide rank sort (bottom) showing divergence score for chimp-biased enhancers (C, red) and human-biased enhancers (D, blue), as well as a shuffled control for each (gray). A close-up of the ranked enhancers at the end of the divergence score spectrum (top 1000, highlighted in pink) is shown on the bottom right.

Cell

Supplemental Information

Enhancer Divergence and *cis*-Regulatory Evolution in the Human and Chimp Neural Crest

Sara L. Prescott, Rajini Srinivasan, Maria Carolina Marchetto, Irina Grishina, Iñigo Narvaiza, Licia Selleri, Fred H. Gage, Tomek Swigut, and Joanna Wysocka

Supplemental Experimental Procedures

IPSC culture

hESCs (H9 line), human iPSCs (WT-33 and ADRC-40) and chimp iPSCs (1209, 0818) were expanded in feeder-free, serum-free medium mTESR-1 from StemCell technologies. Cells were passaged ~1:6 every 5–6 days by incubation with accutase (Invitrogen) and the resulting small cell clusters (50–200 cells) were subsequently re-plated on tissue culture dishes coated overnight with growth-factor-reduced matrigel (BD Biosciences).

CNCC derivation and culture

Pluripotent lines were differentiated into CNCC as previously described (Rada-Iglesias et al., 2012). Briefly, hESCs/iPSCs were incubated with 2mg/ml collagenase. Once detached, clusters of 100-200 cells were plated in CNCC differentiation medium: 1:1 Neurobasal medium/D-MEM F-12 medium (Invitrogen), 0.5× B-27 supplement with Vitamin A (50× stock, Invitrogen), 0.5× N-2 supplement (100× stock, Invitrogen), 20 ng/ml bFGF (Peprotech), 20 ng/ml EGF (Sigma-Aldrich), 5 μg/ml bovine insulin (Sigma-Aldrich) and 1× Glutamax-I supplement (100× stock, Invitrogen). Medium was changed every other day. After seven days of differentiation, neuroepithelial spheres attached to the dish and gave rise to migratory CNCC. Three-four days after the appearance of the first CNCC, cells were dissociated with accutase until single cells and passaged onto fibronectin-coated plates. CNCCs were then transitioned to CNCC early maintenance media: 1:1 Neurobasal medium/D-MEM F-12 medium (Invitrogen), 0.5× B-27 supplement with Vitamin A (50× stock, Invitrogen), 0.5× N-2 supplement (100× stock, Invitrogen), 20 ng/ml bFGF (Peprotech), 20 ng/ml EGF (Sigma-Aldrich), 1 mg/ml bovine serum albumin, serum replacement grade (Gemini Bio-Products # 700-104P) and 1× Glutamax-I supplement (100× stock, Invitrogen). CNCCs were passaged onto fibronectin-coated plates 1:3 every three days, and after 1-2 passages, transitioned to CNCC long term maintenance media, which is composed of CNCC early maintenance media plus 3uM ChIRON

99021 (Selleck, CHIR-99021) and 50ng/ml BMP2 (Peprotech). Cells were maintained on fibronectin with passaging every ~3 days, and collected at passage 4 for all ChIPs and downstream assays. For directed differentiation to later lineages, cells were cultured for seven days in media that promoted differentiation to smooth muscle (D-MEM F-12 + 10% FBS), or neurons/glia (D-MEM F12 + B27 + 2mM glutamine + 50ng/ml BMP2 + 50ng/ml LIF + 1% heat-inactivated serum).

ChIP-seq antibodies

All antibodies used were previously reported as suitable for ChIP and/or ChIP-seq: p300 (sc-585, Santa Cruz Biotechnology), H3K4me1 (ab8895, Abcam), H3K27ac (39133, Active Motif), H3K4me3 (39159, Active Motif), H3K27me3 (39536, Active Motif), NR2F1 (PP-H8132-00, Perseus Proteomics), and TFAP2A (sc-184, Santa Cruz Biotechnology).

Immunocytochemistry

Cells were fixed in fresh 4% paraformaldehyde. For stainings with antibodies recognizing intracellular epitopes, phosphate buffered saline with 0.5 mg/ml BSA and 0.1% Triton X-100 was used for blocking and permeabilization. For cell surface stainings (e.g., p75) TritonX-100 was eliminated from the blocking buffer and cells were additionally methanol-fixed for 10 minutes. Appropriate Alexa 488, or Alexa 594, labeled secondary antibodies and/or DAPI counterstaining was used for visualization on a confocal microscope (Leica TSC SP2).

Xenotransplantation of human and chimp CNCCs into chick embryos

Chick embryos were cultured in a humidified 37°–38°C incubator until HH st. 8-11, then embryos were transferred to weigh trays for injections. Human and chimp CNCCs were transiently transfected with pMAX-GFP, cultured overnight, washed with PBS and injected via mouth pipette under a fluorescent microscope into the dorsal-most portion of the chick neural tube anterior to rhombomere 5. Embryos were then treated with antibiotics and returned to the incubator for 48

hours before dissection to remove extraembryonic tissues and yolk followed by fluorescence imaging. Samples were then frozen and sectioned on a Cryostat at 12uM thickness.

Surface marker identification and analysis

In preliminary work for this study, we observed a level of variation in the transcriptome between different derivations of CNCCs which was obscuring true interspecies differences, which we deemed unacceptable. Scarcity of suitable flow cytometry markers for human CNCCs prompted us to identify in an unbiased fashion a panel of 5 “cluster of differentiation” (CD) antibodies to standardize the culture conditions to promote reproducibility and homogeneity of CNCCs. First, we identified the subsets of significantly expressed genes with highest variance across multiple conditions (high vs low stress, early vs late neural crest) in our RNAseq data, and identified 17 candidate surface marker genes among this group. Due to antibody availability and some redundancies based on gene cluster identities, we further reduced this set to 13 candidate markers and tested each in flow cytometry (AriaII SORP and BD Fortessa) for surface expression and clear dynamic changes during the course of our CNCC derivation from the iPSC/ESC state. Finally we settled on a non-redundant subset of 5 antibodies consisting of CD10 (MME), CD99, CD105 (ENG), CD266 (TNFRSF12A) and CD271 (NGFR, p75) (Miltenyi Biotec) that trace differentiation progress *in vitro*. Of note p75/CD271 is a known marker of neural crest cells and was re-identified in the process. All 5 antibodies were cross-reactive with both species, and were used to assess homogeneity of derived CNCCs.

Analysis of chimpanzee and human enhancer activity in a lacZ reporter transgenic mouse assay

Divergent regulatory regions for CNTNAP2 and PAPPA were chosen for *in vivo* testing in the mouse embryo in a lacZ reporter transgenic assay, as previously described (Ferretti et al., 2011; Vitobello et al., 2011). Briefly, enhancer candidate regions consisting corresponding to chr7: 145,843,942-145,844,366 (hg19) for

the CNTNAP2 enhancer and chr9:118163085-118163446 (hg19) for the PAPPA enhancer and their orthologous chimp sequences respectively were PCR-amplified from genomic DNA using the same primer sets for both species. Three concatenated copies of each fragment were cloned into the hsp68-basal promoter-lacZ reporter vector (DiLeone et al., 1998). Transgenic mouse embryos were generated by pronuclear injection of the relative construct (by Cyagen Biosciences, Santa Clara, CA) (Attanasio et al., 2013; Ferretti et al., 2011; Vitobello et al., 2011) . F0 embryos were collected at E11.5, a time-point that allows evaluation of most developing craniofacial structures and is consistent with other transgenesis analyses of craniofacial enhancers (Attanasio et al., 2013). Embryos were PCR-screened for the presence of the transgene, using primers designed against the lacZ gene, and stained for β-galactosidase activity with 5-bromo-4-chloro-3-indolyl-D-galactopyranoside (X-Gal). Only patterns of craniofacial expression that were observed in at least three different embryos resulting from independent transgenic integration events of the same construct were considered reproducible (Visel et al., 2009). Whole-mount images of all lacZ-positive embryos and close-up images of the heads were taken and expression patterns were annotated according to X-Gal staining of defined anatomical regions.

ATAC-seq

ATAC-seq libraries were performed starting from 50,000 CNCCs from each population, according to published protocols (Buenrostro et al., 2013). Libraries were multiplexed 4 samples per lane and sequenced with 2x50bp paired-end reads.

RNA-seq

Total RNA was extracted from >1x10^6 CNCCs at p4 in Trizol (Invitrogen). 5 µg of total RNA were subjected to two rounds of oligo-dT purification using Dynal oligo-dT beads (Invitrogen), then fragmented with 10× fragmentation buffer (Ambion). Fragmented RNA was used for first-strand cDNA synthesis, using random

hexamer primers (Invitrogen) and SuperScript II enzyme (Invitrogen). Second strand cDNA was obtained by adding RNaseH (Invitrogen) and DNA Pol I (New England Biolabs) to the first strand cDNA mix. The resulting double-stranded cDNA was used for Illumina library preparation as described for ChIP-seq experiments, and sequenced with 2x100bp paired-end reads.

Luciferase reporters

The pGL3-control vector (Promega) was modified to remove the SV40 enhancer. Human and chimp enhancers were amplified from genomic DNA and cloned between the BglII and XhoI sites. Reporter vectors were co-transfected with FuGENE 6 (Promega) into p4 CNCC at a 1:200 ratio with pRL-SV40 renilla luciferase (Promega), and luminescence was measured using the Dual-Luciferase® Reporter Assay System after 24 hours post-transfection. In all cases, the same primers were used to amplify orthologous human and chimp enhancers. Luminescence measurements were repeated for all reporters in three independent CNCC differentiations of each species. For testing the Coordinator motif activity, four versions of the motif were used: V1 = natural sequence with best fit to consensus PWM, 4X: CCCATCTGGTTCCCATTAA; V2 = consensus PWM, 4X: CACATCTGTTTTTAATTAA; V3 = mix of 4 strong versions, V4 = version from strongest H3K27ac-marked enhancer, 4X: GCCTTCTGGTTTTAATAAC; empty = empty pGL3 vector.

ChIP-seq analysis and identification of modal peak positions

All sequencing reads were aligned to both reference genomes (hg19 and panTro3) using default settings with bowtie2.2.4, regardless of species of origin. ATAC-seq was paired-end sequenced, Nextera adapter sequence was trimmed away and each mate was treated as independent transposition events for downstream analysis. Wig files for genome browser visualization were generated with QuEST2.4. Peak calls were performed using default settings on MACS2. To generate the list of candidate genomic regions with robust coordinates in both assemblies, we applied the following strategy: for each reference genome,

summit positions from p300, AP2A, NR2F1 ChIPs and ATAC-seq were assigned unique names and combined in one file. LiftOver (-minMatch=0.1 -multiple) was used to map each peak to the reciprocal reference genome. Peak positions in each genome assembly (both original and remapped) where then combined into a single file, sorted on unique names and combined in one table by full outer join. Peaks that could not be mapped by liftOver received a “chr0” placeholder chromosome with numerical coordinates of the original genome. Next we used a mean shift algorithm in two dimensions with a Gaussian kernel of 300bp bandwidth to cluster the peaks into candidate regulatory regions (hence incorporating evidence from both genome coordinates simultaneously). Of note, at our depth of sequencing (~50M reads per sample), using ATAC-seq data only would miss 45% of the putative enhancer sites, while incorporating ATAC-seq to the p300 and TF data increases the number of discovered sites by 20%. For motif analysis we restricted the region set further by identifying regions with bijective (1-to-1) orthology down to the single-base level by repeating liftOver on the ±100bp regions relative to the mean-shift modal peak position, excluding elements whose peripheral (±100bp) coordinates did not remap to the expected coordinates in both species.

Overlaps of genomic intervals with annotated genomic features such as HARs, repetitive elements and VISTA enhancers were calculated using Bedtools and statistical analysis was performed with Fisher’s exact test followed by q-value calculation (using a Storey-Tibshirani procedure). HAR coordinates were found in Hubisz and Pollard, 2014, and repeat coordinates and classifications were extracted from the UCSC genome browser repeat masker track. VISTA enhancer coordinates are available from the VISTA database

RNA-seq analysis and enhancer association

RNA-seq were aligned to hg19 and panTro3 reference genomes with tophat and quantified against human ENSEMBL 78 (GRCh37) gene models using htseq-count. Differential expression analysis was performed with DESeq2. To assign most likely target genes for the regions identified in ChIP-seq we applied default

GREAT association rules (McLean et al., 2010). To calculate the effect of multiple enhancers, all enhancers from either species were scored as 0 (invariant, p > .0001), +1 (human-biased p-value < .0001) or -1 (chimp biased p-value < .0001) in hg19. Genes with divergent gene expression (padj <0.1) are then binned by the cumulative count of all enhancers within 250kb of the TSS and violin plots were generated in Matlab for the log(fold change human/chimp) of expression according to DESeq2.

Conservation plots

Conservation plots were generated using the Conservation Plot (version 1.0.0) tool available through Galaxy/Cistrome.

Variance-edit distance

To estimate the effect of genetic distance on divergence of epigenetic marks we binned the chromatin regions based on Levenshtein distance of the 200bp orthologous regions and calculated variance of pairwise difference in the ChIP signal for each alignment within each Levenshtein distance bin. For plotting purpose the variances were normalized to that of distance=0 by subtracting the variance at zero distance.

Similarity with other datasets

To assess similarity with other human cell types, we downloaded over 50 H3K27ac public ChIP-seq datasets from a representative set of cell types. The kernel density estimate was calculated at approximately 50,000 genomic regions based on the superset of ENCODE transcription factor ChIP-seq data, DNase hypersensitivity and our own datasets. (1-Spearman correlation coefficient) was used as metric for clustering. Since no epigenomic data from *in vivo* human CNCCs are available, we calculated correlation coefficients for the portion of sites defined above that were remappable to the chick genome with H3K27ac ChiP-seq data from neural crest from HH stage 20 chick facial prominence (SRX148743, Rada Iglesias et al.).

Pleiotropic Versus CNCC-specific motif enrichment

CNCC enhancers were classified as increasingly pleiotropic by scoring for H3K27ac ChIP-seq enrichments from 30 public data set cell types and binned by number of tissues with activity (1 to 31). The fraction of enhancers per bin with recognizable Coordinator motif was calculated using FIMO with p-value cutoff < 0.0001.

Motif discovery

Enriched and *de novo* motif discovery was performed using SeqPos tool in Cistrome with the top 1904 active enhancers as well as with top 3499 CNCC-specific enhancers. To analyze motif usage in the annotated set of genomic regions, we considered approximately 200,000 x 200bp intervals (centered at the summits) with bijective orthology at the base resolution (as defined above). Fasta files were then generated from hg19 and panTro3 reference genomes corresponding to the set of genomic regions, and scanned for motifs with FIMO using combined MEME Jolma2013 and Jaspar core 2014 vertebrates databases plus de novo motifs at cutoff of $p<0.0001$. To detect motif instances that have changed between species, the full outer join of the fimo outputs was performed with missing matches assigned conservatively a p-value of 0.005. The log ratio of the p-values for orthologous motifs was calculated and used in downstream analyses. In addition, the odds ratio and p-value for enrichment at biased sites was calculated with Fisher's exact test.

To determine which motifs might have functional input into chromatin modifications in CNCCs, we calculated a correlation coefficient per motif between the log ratio p-value for its PWM and log ratio of chromatin feature signal at all sites containing the motif with discoverable species bias genome-wide. For visualization, the resulting matrix was bi-clustered with heatmap.2 and fastcluster functions in R.

For selected motifs we used the experimental information on the strength of the allele (H3K27ac enrichment) to further resolve which particular nucleotide

mutations within the motif are favored at the stronger allele/ortholog. For each motif we tabulated mutations present in the strong allele and the resulting PWM was visualized with SeqLogo. As a control, the same analysis was performed for the weak allele/ortholog.

Sequence comparison with ancestral outgroups

To identify directionality of evolutionary changes at Coordinator sites we calculated p-value scores with FIMO at orthologous human, chimp and human-chimp ancestor sequence inferred by the ENSEMBL EPO pipeline. To visualize changes we plotted -log10 p-values for each of three reference genomes and for subsets of enhancers as orthographic projections along space diagonal. The sequences of Neanderthal (Altai) and Denisova individual were obtained from Max Planck Institute for Evolutionary Anthropology server. (Meyer et al.2012; Prüfer et al., 2014).

Calculation of divergence score and identification of clusters of regulatory divergence

All enhancers with 1-to-1 orthology were assigned a p-value corresponding to species divergence of H3K27ac enrichment (see details above). To calculate a divergence score, enhancers with human bias (p-value<0.1) and, separately, enhancers with chimp bias (p-value <0.1) were sorted by chromosomal position in hg19. For each sorted enhancer, the –log10(p-value) of the closest 8 enhancers (with q<0.1 bias toward the same species, in either chromosomal direction) was summed, and divided by the distance (bp) between the centers of the two furthest (±8) enhancers. To estimate background distributions, the analysis was repeated after p-values of species bias were randomly reassigned across all enhancers. To consolidate into distinct clusters and distinguish the boundaries of the regions, the window of integration (from the start of the -8 enhancer to the end of the +8 enhancer) for all enhancers with a divergence score over 2.5×10^{-4} were merged using Bedtools. Association with genes was done using GREAT default settings. All plots were generated in Matlab.

Supplemental References

Ferretti, E., Li, B., Zewdu, R., Wells, V., Hebert, J.M., Karner, C., Anderson, M.J., Williams, T., Dixon, J., Dixon, M.J., et al. (2011). A Conserved Pbx-Wnt-p63-Irf6 Regulatory Module Controls Face Morphogenesis by Promoting Epithelial Apoptosis. Dev. Cell *21*, 627–641.

Meyer, M., Kircher, M., Gansauge, M.-T., Li, H., Racimo, F., Mallick, S., Schraiber, J.G., Jay, F., PrJ.G., K., de Filippo, C., et al. (2012). A high-coverage genome sequence from an archaic Denisovan individual. Science *338*, 222ce a

Prüfer, K., Racimo, F., Patterson, N., Jay, F., Sankararaman, S., Sawyer, S., Heinze, A., Renaud, G., Sudmant, P.H., de Filippo, C., et al. (2014). The complete genome sequence of a Neanderthal from the Altai Mountains. Nature *505*, 43ure

Rada-Iglesias, A., Bajpai, R., Prescott, S., Brugmann, S.A., Swigut, T., and Wysocka, J. (2012). Epigenomic annotation of enhancers predicts transcriptional regulators of human neural crest. Cell Stem Cell *11*, 633–648.

Visel, A., Minovitsky, S., Dubchak, I., and Pennacchio, L.A. (2007). VISTA Enhancer Browser--a database of tissue-specific human enhancers. Nucleic Acids Res. *35*, D88–D92.